PREDICTION OF GROUND MOTIONS

FOR THRUST EARTHQUAKES

by

Paul Somerville

Woodward-Clyde Federal Services
Pasadena, California

and

Norman Abrahamson

Castro Valley, California

Data Utilization Report CSMIP/00-01 (OSMS 00-03)

California Strong Motion Instrumentation Program

February 2000

CALIFORNIA DEPARTMENT OF CONSERVATION
DIVISION OF MINES AND GEOLOGY
OFFICE OF STRONG MOTION STUDIES

THE RESOURCES AGENCY
MARY NICHOLS
SECRETARY FOR RESOURCES

STATE OF CALIFORNIA
GRAY DAVIS
GOVERNOR

DEPARTMENT OF CONSERVATION
DARRYL YOUNG
DIRECTOR

DIVISION OF MINES AND GEOLOGY
JAMES F. DAVIS
STATE GEOLOGIST

DISCLAIMER

The content of this report was developed under Contract No. 1093-553 from the Strong Motion Instrumentation Program in the Division of Mines and Geology of the California Department of Conservation. This report has not been edited to the standards of a formal publication. Any opinions, findings, conclusions or recommendations contained in this report are those of the authors, and should not be interpreted as representing the official policies, either expressed or implied, of the State of California.

PREDICTION OF GROUND MOTIONS

FOR THRUST EARTHQUAKES

by

Paul Somerville

Woodward-Clyde Federal Services *
Pasadena, California

and

Norman Abrahamson **

Castro Valley, California

Data Utilization Report CSMIP/00-01 (OSMS 00-03)

California Strong Motion Instrumentation Program

February 2000

* Now URS Greiner Woodward Clyde.
** Now at Pacific Gas & Electric Company, San Francisco.

This study was conducted at Woodward-Clyde Federal Services in Pasadena, California from June 1994 to December 1995, and was supported by the Department of Conservation under Contract No. 1093-553.

California Department of Conservation
Division of Mines and Geology
Office of Strong Motion Studies
801 K Street, MS 13-35
Sacramento, California 95814-3531

PREFACE

The California Strong Motion Instrumentation Program (CSMIP) in the Division of Mines and Geology of the California Department of Conservation promotes and facilitates the improvement of seismic codes through the Data Interpretation Project. The objective of the this project is to increase the understanding of earthquake strong ground shaking and its effects on structures through interpretation and analysis studies of CSMIP and other applicable strong motion data. The ultimate goal is to accelerate the process by which lessons learned from earthquake data are incorporated into seismic code provisions and seismic design practices.

The specific objectives of the CSMIP Data Interpretation Project are to:

1. Understand the spatial variation and magnitude dependence of earthquake strong ground motion.

2. Understand the effects of earthquake motions on the response of geologic formations, buildings and lifeline structures.

3. Expedite the incorporation of knowledge of earthquake shaking into revision of seismic codes and practices.

4. Increase awareness within the seismological and earthquake engineering community about the effective usage of strong motion data.

5. Improve instrumentation methods and data processing techniques to maximize the usefulness of SMIP data. Develop data representations to increase the usefulness and the applicability to design engineers.

This report is part of CSMIP data utilization reports designed to transfer recent research findings on strong-motion data to practicing seismic design professionals and earth scientists. CSMIP extends its appreciation to the members of the Strong Motion Instrumentation Advisory Committee and its subcommittees for their recommendations regarding the Data Interpretation Research Project.

Anthony F. Shakal
CSMIP Program Manager

Moh J. Huang
CSMIP Data Interpretation
Project Manager

PREDICTION OF GROUND MOTIONS FOR THRUST EARTHQUAKES

ABSTRACT

The peak accelerations recorded on alluvial sites during the Northridge earthquake were about 50% larger than the median value predicted by current empirical attenuation relations at distances less than about 30 km. This raises the question of whether the ground motions from the Northridge earthquake are anomalous for thrust events, or are representative of ground motions expected in future thrust earthquakes. Since the empirical data base contains few strong motion records close to large thrust earthquakes, it is difficult to assess whether the Northridge ground motions are anomalous based on recorded data alone. We have used a broadband strong motion simulation procedure to help assess whether the ground motions were anomalous. The ground motions from the Northridge earthquake and our simulations of these ground motions have a similar pattern of departure from empirical attenuation relations for thrust earthquakes: the peak accelerations are at about the 84th percentile level for distances within 20 to 30 km, and follow the median level for larger distances. This same pattern of departure from empirical attenuation relations was obtained in our simulations of the peak accelerations of an Elysian Park blind thrust event prior to the occurrence of the Northridge earthquake, and from twenty randomly generated rupture models of future Northridge earthquakes. Since we are able to model this pattern with broadband simulations, and had done so before the Northridge earthquake occurred, this suggests that the Northridge strong motion records are not anomalous, and are representative of ground motions close to thrust faults. Accordingly, it seems appropriate to include these recordings in strong motion data sets that are used to develop empirical ground motion attenuation relations for thrust faults, and to use this augmented data set as the basis for evaluating the need for modifications in design coefficients in the seismic provisions of building codes.

We evaluated systematic differences in ground motion on the hanging wall and foot wall during the Northridge earthquake using empirical data. An empirical model for the hanging wall effect was developed for the Northridge earthquake. This empirical model results in up to a 50% increase in peak horizontal accelerations on the hanging wall over the distance range of 10 to 20 km relative to the median attenuation for the Northridge earthquake. In

contrast, the peak accelerations on the foot wall are not significantly different from the median attenuation over this distance renge. Recordings from other reverse events show a similar trend of an increase in the peak accelerations on the hanging wall, indicating this systematic difference in hanging wall peak accelerations is likely to be observed in future reverse events.

A modification to the near source factor in the proposed 1997 revisons to the Uniform Bulding Code is proposed to accommodate hanging wall effects near crustal thrust faults in California.

APPLICATION TO CODES AND PRACTICES

The current version of the Uniform Building Code (1994 Edition) does not include any adjustments for near fault conditions. In Zone 4 (which includes most of California) it specifies that the short-period spectral acceleration is limited to 1.0g for soil type II. The revisions to the UBC for 1997 proposed by the Structural Engineers' Association of California includes a near source factor N. The proposed values of this factor, which are a function of distance and of the capability of the fault to produce large earthquakes (Table A-1), are given in Table A-2, which includes Tables 16-S and 16-T of the proposed revised code. The intention of the N factor is to accommodate larger ground motion levels near large earthquakes, especially those due to rupture directivity effects at longer periods, which are well documented in the recorded data and described by empirical attenuation relations. The N factor causes a period-independent scaling of the ground motions.

The largest increase provided for in the proposed revised code is a factor of 1.9, which would produce a short-period spectral acceleration of 1.9g. The ground motions recorded in the near source region during the Northridge earthquake exceeded these levels. Naeim (1995) compares these recorded motions to the current (1994) UBC and discusses design approaches that may be effective for controlling the effects of large near-fault ground motions.

As seen from Table A-2, the near source factor N becomes unity at distances of 10 km and larger. However, as we show in our study, ground motions recorded on the hanging wall during the Northridge earthquake in the distance range of 10 to 20 km caused ground motions to be up to 50% larger than the median ground motion level for the earthquake. This suggests that the near source factor needs to be extended to larger distances on the hanging wall of thrust faults.

In Table A-3 we provide a set of revised distance ranges and N factors that would accommodate hanging wall effects. Our N factor for seismic source type B has been raised from 1.2 to 1.4 because we do not expect the hanging wall effect to be strongly dependent on magnitude as is implied by the definition of seismic source types A, B and C. Crustal thrust faults in California have slip rates corresponding to seismic source types B and C, and our data

for the hanging wall effect are from earthquakes in the magnitude range of 6 to 7.4.

An additional adjustment factor of 1.3 for thrust and reverse faults relative to strike-slip faults is suggested by current empirical attenuation relations, and the Northridge earthquake implies that for some earthquakes the factor may be closer to 1.5. However, if we consider that the current code applies to the average of strike-slip and thrust or reverse faults, a factor of 1.14 to 1.22 on either side of this average, while certainly relevant in a site-specific ground motion evaluation, may be too much refinement for a building code. Nevertheless, the presence of this additional factor serves to emphasize the need for the hanging wall factor that we propose.

Table A-1. Seismic Source Type in Current Code Revision

(Reproduction of Table 16-T - SEISMIC SOURCE TYPE; SEAOC - UBC Strength Design, Draft 10/11/95)

Seismic Source Type	Seismic Source Description	Seismic Source Definition	
		Maximum Moment Magnitude, M	Slip Rate, SR (mm/year)
A	Faults that are capable of producing large magnitude events and which have a high rate of seismic activity	and $M \geq 7.0$	$SR \geq 5$
B	All faults other than Types A and C		
C	Faults which are not capable of producing large magnitude earthquakes and which have a relatively low rate of seismic activity	and $M < 6.5$	$SR \leq 2$

Table A-2. Near Source Factor in Current Code Revision

(Reproduction of Table 16-S NEAR SOURCE FACTOR N; SEAOC - UBC Strength Design, Draft 10/11/95)

Seismic Source Type	Closest Distance to Seismic Source[1,2]		
	≤ 2 km	5 km	≥ 10 km
A	1.9	1.5	1.0
B	1.5	1.2	1.0
C	1.0	1.0	1.0

1. The location and type of seismic sources to be used for design shall be established by the building official or based on approved geotechnical data.

2. The closest distance to seismic source shall be taken as the minimum distance between the site and the area described by the vertical projection of the source on the surface (i.e., surface projection of fault plane). The surface projection need not include portions of the source at depths of 7.5 km, or greater. The largest value of the near-source factor of sources shall be used for design.

3. The near-source factor may be based on the linear interpolation of values for distances other than those shown in the table. Alternatively, the value of N for Type A faults may be calculated as $N = 2.13 - 0.113d_f$, and the value of N for Type B faults may be calculated as $1.7 - 0.1d_f$, where d_f = the closest distance to fault rupture. In all cases, N shall not be taken as less than 1.0.

Table A-3. Proposed Change to Near Source Factor in Current Code Revision

Table 16-Sa NEAR SOURCE FACTOR N FOR STRIKE-SLIP FAULTS AND THE FOOT WALL OF DIPPING FAULTS

Seismic Source Type	Closest Distance to Seismic Source[1,2]		
	≤ 2 km	5 km	≥ 10 km
A	1.9	1.5	1.0
B	1.5	1.2	1.0
C	1.0	1.0	1.0

1. The location and type of seismic sources to be used for design shall be established by the building official or based on approved geotechnical data.

2. The closest distance to seismic source shall be taken as the minimum distance between the site and the area described by the vertical projection of the source on the surface (i.e., surface projection of fault plane). The surface projection need not include portions of the source at depths of 7.5 km, or greater. The largest value of the near-source factor of sources shall be used for design.

3. The near-source factor may be based on the linear interpolation of values for distances other than those shown in the table. Alternatively, the value of N for Type A faults may be calculated as $N = 2.13 - 0.113d_f$, and the value of N for Type B faults may be calculated as $1.7 - 0.1d_f$, where d_f = the closest distance to fault rupture. In all cases, N shall not be taken as less than 1.0.

Table 16-Sb NEAR SOURCE FACTOR N FOR THE HANGING WALL OF DIPPING FAULTS

Seismic Source Type	Closest Distance to Seismic Source[1,2]		
	≤ 2 km	5-20 km	≥ 30 km
A	1.9	1.5	1.0
B	1.5	1.4	1.0
C	1.0	1.0	1.0

3. The near-source factor may be based on the linear interpolation of values for distances other than those shown in the table.

ACKNOWLEDGMENTS

Strong motion data were provided by the Dr Moh Huang of the California Strong Motion Instrumentation Program, the United States Geological Survey, Professor M. Trifunac of the University of Southern California, and Mr Ron Tognazzini of the Los Angeles Department of Water and Power. Ground motion modeling and analyses were performed by James McLaren and Nancy Smith.

PREDICTION OF GROUND MOTIONS FROM THRUST EARTHQUAKES

TABLE OF CONTENTS

CHAPTER 1. IMPLICATIONS OF THE NORTHRIDGE EARTHQUAKE FOR STRONG GROUND MOTIONS NEAR THRUST FAULTS

Introduction

As a result of the large number of strong motion instruments deployed throughout the greater Los Angeles region, the Northridge earthquake produced the largest set of strong motion recordings ever obtained from a large thrust earthquake. This data set contains some of the largest strong motions ever recorded. The peak accelerations from the Northridge earthquake recorded on alluvium were about 50% larger (about one standard deviation larger) than the median value predicted by current empirical attenuation relations at distances less than about 30 km (Campbell, 1995), as illustrated in Figure 1-1a. Distance is measured as the closest distance from the recording site to the inferred rupture plane of the earthquake. Since the Northridge earthquake was widely recorded on strong motion instruments, and had a very large societal impact because of its occurrence in a densely populated urban community, it may have a strong influence on the development of empirical ground motion attenuation relations, and on the revision of seismic provisions in building codes. For this reason, it is important to determine whether the ground motions from the Northridge earthquake are anomalous for thrust events, or if they are representative of ground motions expected in future thrust earthquakes.

Following the occurrence of the 1987 Whittier Narrows earthquake on an inferred blind thrust fault, we used the strong motion simulation procedure described below to predict peak accelerations from a magnitude 7 blind thrust earthquake on the hypothesized Elysian Park blind thrust (Saikia, 1993). The depth ranges of faulting of the Elysian Park model and the Northridge earthquake are very similar: 8 to 20 km for the Elysian Park thrust simulation and 7.5 to 20 km for the Northridge earthquake. The assumed dip of 30 degrees for the Elysian Park thrust was somewhat shallower than the 42 degree dip of the Northridge earthquake. The simulated peak accelerations for soft rock or stiff alluvial conditions for the Elysian Park event, shown in Figure 1-1b, lie at about the 84th percentile of the empirical attenuation

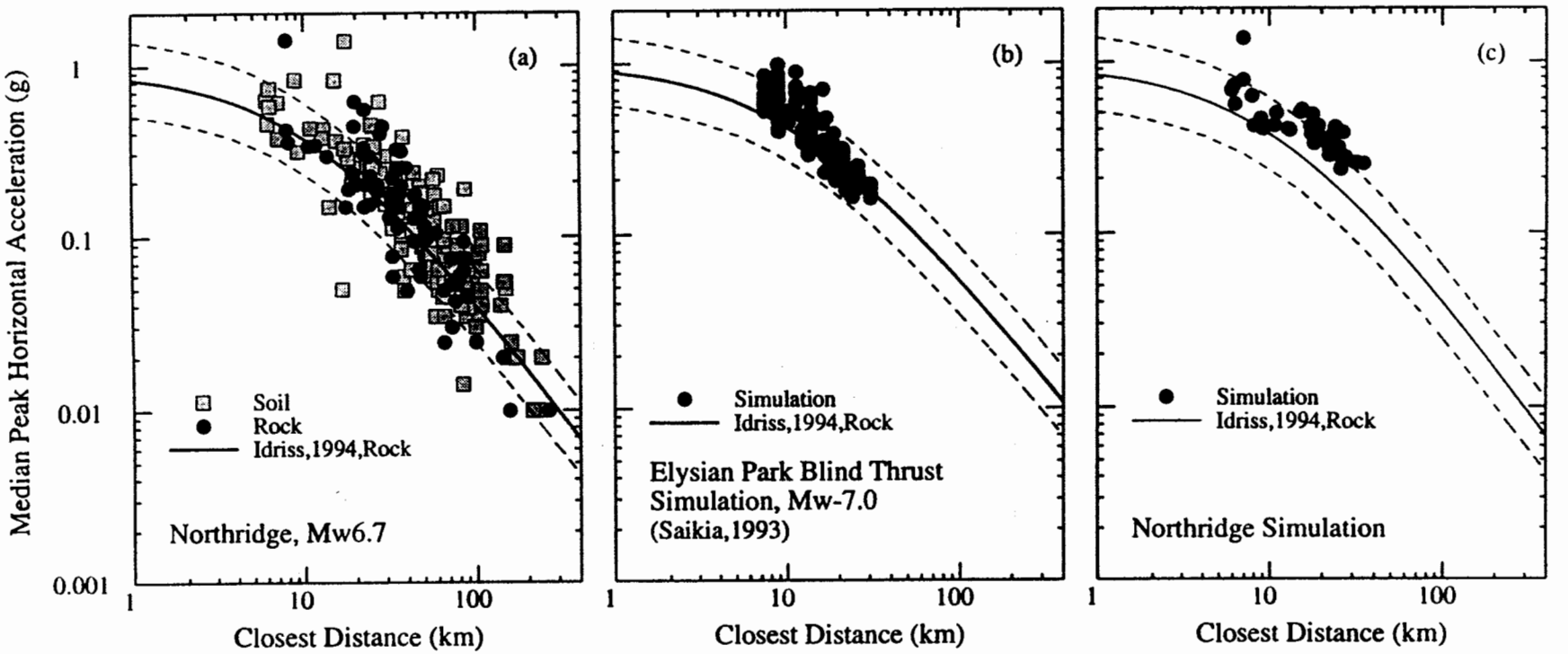

Figure 1-1. (a). Comparison of recorded peak accelerations from the Northridge earthquake with the attenuation relation of Idriss (1991) for thrust earthquakes recorded on rock and stiff soil as a function of closest distance to the inferred rupture surface. (b). Comparison of simulated peak accelerations for a M_w 7 earthquake on the Elysian Park blind thrust (Saikia, 1993) with the relation of Idriss (1991). (c). Simulations using the Northridge rupture model of Wald and Heaton (1994) compared with the Idriss (1991) relation.

relation for distances closer than about 20 km, and at about the median empirical attenuation relation for distances larger than 20 km. This pattern is similar to that of the peak accelerations recorded during the Northridge earthquake, as shown in Figure 1a.

The simulation procedure has been validated against a large body of strong motion data from California earthquakes, and so we expect it to produce accurate estimates of ground motions for any given rupture scenario, including blind thrust events such as the Elysian Park event for which no good precedent existed in the strong motion data base until the occurrence of the Northridge earthquake. The close agreement between our pre-Northridge estimates for the Elysian Park scenario event and the ground motions recorded during the Northridge earthquake in effect constitutes a blind test validation of the simulation procedure. In this chapter, we use this broadband ground simulation procedure to assess whether the strong motions recorded during the Northridge earthquake are anomalous, or whether thay are representative of ground motions expected near thrust faults.

Broadband Strong Motion Modeling Procedure

The rupture model of the Northridge earthquake described below was derived from strong motion data in a frequency range (less than 1 Hz) in which we are able to model the waveforms of the recorded ground motions. In this frequency range, we can use deterministic models of earthquake source and wave propagation phenomena to explain the recorded motions. However, as frequencies increase above 1 Hz, the amplitudes and waveforms of strong ground motions become increasingly stochastic in nature, and we are unable to model them using deterministic source and path models. This necessitates the use of two separate procedures for the computation of broadband seismograms.

The broadband ground motion simulation procedure that we use is a hybrid procedure that computes the low frequency and high frequency ranges separately and then combines the two to produce a single time history. At frequencies below 1 Hz, it contains a theoretically rigorous representation of radiation pattern, rupture directivity and wave propagation effects,

and reproduces recorded ground motion waveforms and amplitudes. At frequencies above 1 Hz, it uses a theoretically rigorous representation of wave propagation effects which is combined with theoretically-based semi-empirical representations of stochastic aspects of the source radiation, scattering in the path and site, and the receiver function. The simulation procedure has been calibrated against the recorded strong motions from numerous earthquakes.

The synthetic seismogram procedure that we use to generate the low frequency part of the broadband seismogram is described by Hartzell and Heaton (1983). It is implemented using frequency-wavenumber integration to compute Green's functions which are convolved with the slip function on the fault. The high frequency ground motion simulation procedure that we use is described by Wald et al. (1988a) and Somerville (1993). It is implemented using a generalized ray method to calculate simplified Green's functions, which are convolved with empirical source functions derived from near-fault strong motion recordings of small earthquakes.

The fault model is specified as a finite rectangular fault surface that is divided into discrete sub-fault elements, and the motions from these elements are summed and lagged to simulate the propagation of rupture over the fault surface. The parameters required for specifying the source are seismic moment, fault length, fault width, strike, dip, rake, depth of top of fault, hypocenter, rupture velocity, and slip distribution (which may include spatially variable rake and time function of slip). Radiation pattern and fault subevents are treated differently in the two frequency ranges. At low frequencies (<1 Hz), the fault is discretized finely enough to produce a continuous slip function for frequencies below one second, and the theoretical radiation pattern is used. At high frequencies (>1 Hz), the fault is discretized into sub-fault elements having dimensions of several km. The radiation of seismic waves from these sub-fault elements is represented by empirical source functions, which are recorded accelerograms of events having the dimensions of the fault elements (magnitude ~ 5 earthquakes) that have been corrected back to the source using simplified Green's functions calculated as described below. The radiation pattern is represented empirically by selecting source functions having the required theoretical radiation pattern value for each sub-fault

element. We have used empirical source functions derived from aftershocks of the 1979 Imperial Valley and 1987 Whittier Narrows earthquakes.

The modeling of wave propagation effects requires the specification of seismic velocities, density, and damping coefficient (expressed by Q) of a flat layered crustal model. Path effects are treated differently in the two frequency ranges. At low frequencies (<1 Hz), path effects are represented by Green's functions calculated using an efficient frequency-wavenumber integration scheme (Saikia, 1994a). These Green's functions contain the complete response of the anelastic layered medium (all body wave and surface wave phases) for frequencies below a given value (typically chosen to be 5 Hz). They contain the near-field term in addition to the far-field term, and include the static displacement field of the earthquake. At high frequencies (>1 Hz), path effects are represented by simplified Green's functions calculated using generalized ray theory (Helmberger and Harkrider, 1978). These Green's functions are accurate up to indefinitely high frequencies (typically 50 Hz), and contain all of the significant rays. They are simplified in the sense that they do not include the radiation pattern and the receiver function. The simplified Green's functions are used to transfer the empirical source functions from the depth, horizontal range and velocity structure in which they were recorded to the depth, horizontal range and velocity structure in which they are to be used for ground motion simulation.

At low frequencies, site effects are incorporated by calculating Green's functions using surface velocity, density and Q appropriate for the site. For the high frequency part of the simulation, the receiver function is included empirically in the empirical source functions; the partitioning of energy among components is treated in a site-specific manner by applying a receiver function correction to the empirical source functions which rotates the recorded wave field into the appropriate partitioning for the velocity structure at the site. Scattering effects near the site are represented by wave propagation effects contained in the empirical source functions that are not modeled by the simplified Green's functions. For this study, we have assumed that the site attenuation contained in the empirical source functions is appropriate for all recording sites, and have not made adjustments for specific sites.

The ground motion model has no free parameters when used to model the recorded ground motions of a past earthquake, and hence no calibration of the model is required. The method has been validated against the recorded strong ground motions of the following earthquakes: 1978 Tabas (Saikia, 1994b); 1979 Imperial Valley (Wald et al., 1988a); 1985 Michoacan, Mexico and Valparaiso, Chile (Somerville et al., 1991a); 1987 Whittier Narrows (Wald et al., 1988b; Saikia, 1993); 1988 Saguenay (Somerville et al., 1990; Atkinson and Somerville, 1994); 1989 Loma Prieta (Somerville et al., 1994a,b); 1994 Northridge (Somerville et al., 1995a 1996; and this report). Based on this extensive validation experience, we have documented that the ground motion simulation procedure is applicable for magnitudes in the range of 5 to 8; distances from 0 to 200 km, and frequencies between 0.2 and 35 Hz.

The uncertainty in ground motions predicted by the model is characterized by the procedure described by Abrahamson et al. (1990) using comparison of recorded and simulated motions. For recent well recorded earthquakes, including the 1989 Loma Prieta (Somerville et al., 1994b) and 1994 Northridge earthquakes (Somerville et al., 1995a, 1996; and this report), the model predicts the recorded ground motions with little or no significant bias and with a standard error of a factor of about 1.4 in the frequency range of 0.2 Hz to 35 Hz.

Rupture Model of the Northridge Earthquake

To model the recorded ground motions of the Northridge earthquake using the simulation procedure requires information on the seismic source, including seismic moment, source geometry and mechanism, hypocenter location, slip distribution, rupture velocity and rise-time. A rupture model, shown in Figure 1-2, was derived by Wald and Heaton (1994) by inverting strong motion data. Rupture began at a depth of 19 km below the surface, and propagated up dip toward the north on a plane dipping at about 42 degrees. The rupture plane has a length along strike of about 18 km and an up dip width of about 21 km; its surface projection is shown in Figure 1-3 together with the locations of strong motion stations. The depths of the bottom (southwest) and top (northeast) edges of the rupture plane are about 20 km and 7.5 km respectively, with most of the rupture confined to depths of 12 km or more.

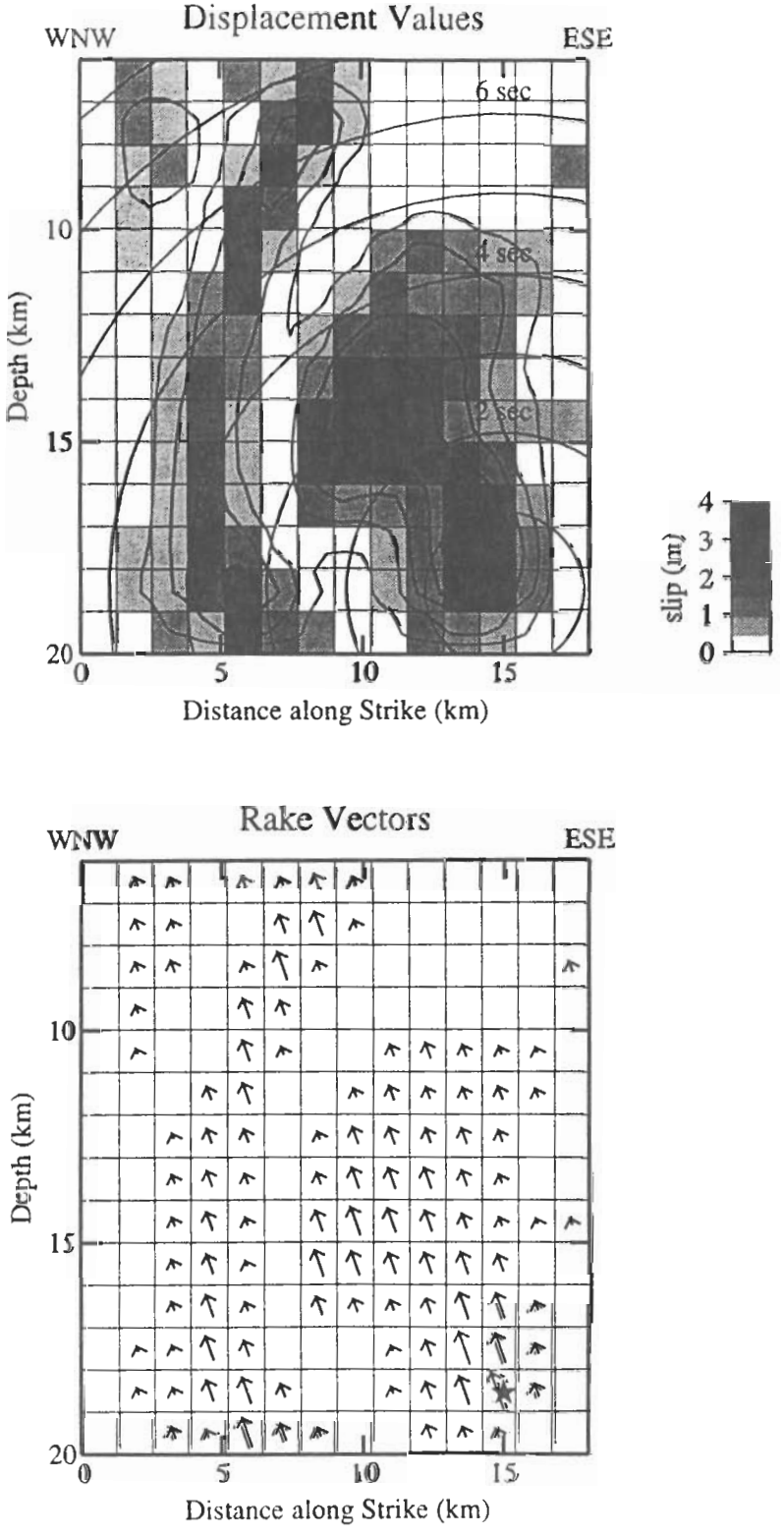

Figure 1- 2. Rupture model of the Northridge earthquake. Source: Wald and Heaton (1994).

Additional rupture models were subsequently derived by Wald et al. (1996) that used teleseismic and geodetic data in addition to strong motion data. The revised rupture model based on strong motion data is quite similar to the model of Wald and Heaton (1994) that we use here.

In calculating Green's functions for the simulation procedure, we used the velocity model that was employed by Wald and Heaton (1994) in generating the rupture model of the earthquake. The ground motion simulations therefore do not take variations in site response into account. In Figure 1-4, we show that the attenuation relations for peak acceleration and peak velocity for soil and rock sites derived from the Northridge data are very similar (Abrahamson and Somerville, 1996). However, we have restricted our analyses to soil sites listed in Table 1-1 of Somerville et al. (1996) to minimize the influence of variations in site response on our results.

Comparison Between Broadband Simulations and Recorded Data

We have used the broadband simulation procedure and the rupture model of the Northridge earthquake described above to simulate the ground motions of the Northridge earthquake at strong motion recording stations. In this section, we compare the simulated strong motions with those that were recorded at near-fault stations on soil shown in Figure 1-3. These recordings are from the strong motion networks of the California Strong Motion Instrumentation Program (Shakal et al., 1995), the United States Geological Survey (Porcella et al., 1995), the University of Southern California (Trifunac et al., 1995), and the Los Angeles Department of Water and Power (Tognazzini et al., 1995). We first make comparisons of peak accelerations and waveforms, then compare the response spectra, and finally compare the durations. As indicated in the description of the simulation procedure, there are no free parameters in the simulation procedure when it is used to simulate the motions of an earthquake for which a rupture model has been determined, and so our simulations of the Northridge earthquake contain no calibration factors.

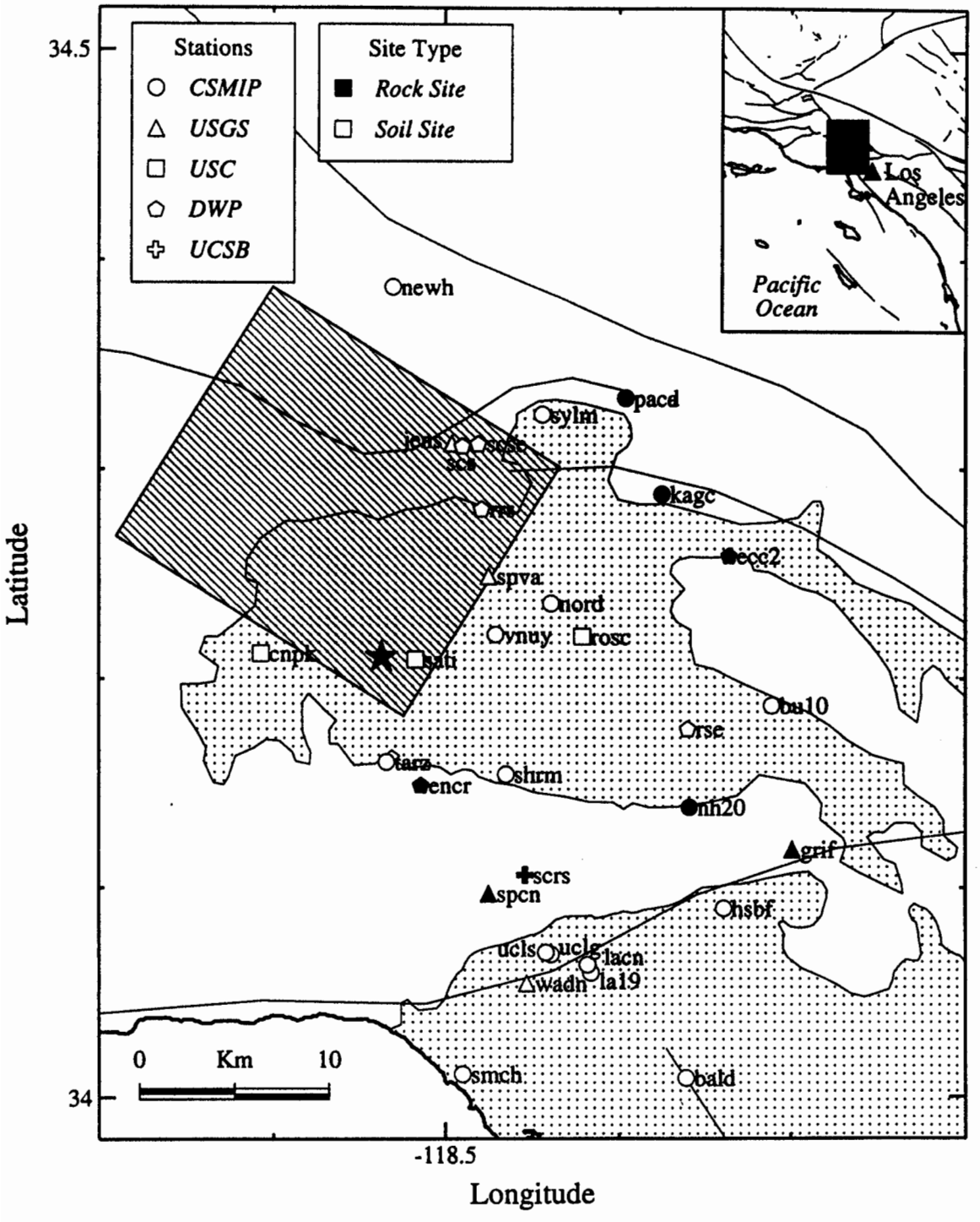

Figure 1-3. Map of strong motion recording stations in the San Fernando Valley and the northwestern Los Angeles Basin, and the surface projection of the rupture plane of the Wald and Heaton (1994) model.

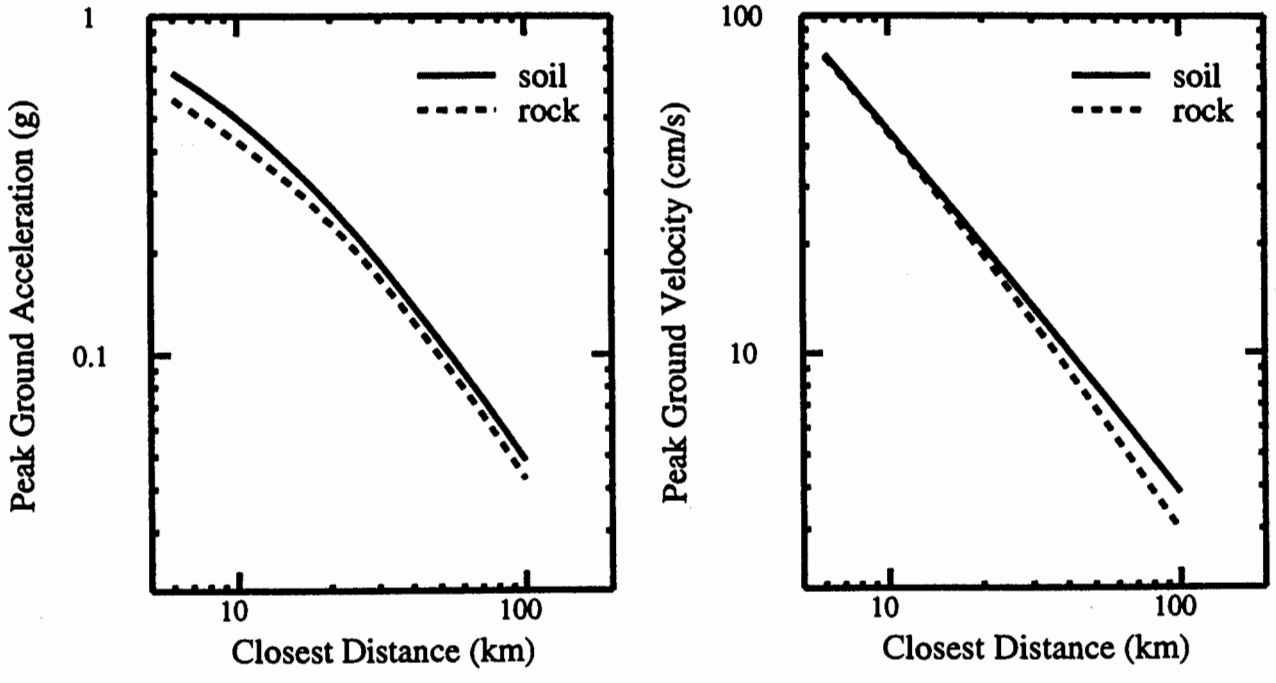

Figure 1-4. Attenuation of peak acceleration and peak velocity at soil and rock sites from the Northridge earthquake. Source: Abrahamson and Somerville (1996).

The peak accelerations generated by the simulation procedure are compared with the recorded peak accelerations in Figures 1-1c and 1-1a. The simulated peak accelerations display a pattern of exceedance of the empirical attenuation relation that is similar to that seen in the data. In general, the simulated ground motion time histories show a fairly close resemblance to the waveforms of the recorded motions at low frequencies. This is as expected since the rupture model was derived from the lowpass filtered strong motion waveforms. To make a qualitative comparison of recorded and simulated waveforms, we compare the recorded three component time histories at Arleta (top row) with those simulated using empirical source functions derived from the Whittier Narrows aftershock (center row) and the Imperial Valley aftershock (bottom row of each panel) in Figure 1-5. The recorded and simulated displacement waveforms have considerable resemblance, especially on the north and east components. There is even more resemblance between the recorded and simulated velocity waveforms, especially in the lower frequency features. The differences between recorded and simulated peak horizontal velocity lie in the range of 15 to 40%. At high frequencies, there is little resemblance in waveform between the recorded and simulated motions, as seen in comparing the recorded and simulated time histories. However, there is resemblance in the duration of the strong motion, which we quantify below.

For most engineering purposes, the most relevant ground motion parameter for comparison between the recorded and simulated motions is the 5% damped response spectral acceleration. The recorded and simulated response spectra at Arleta are compared in Figure 1-6. To make a quantitative comparison, we use the procedure of Abrahamson et al. (1990) to measure the goodness of fit of response spectral acceleration and duration between the recorded and simulated ground motions. The goodness of fit measurement is characterized by two parameters: the bias and the standard error. In this formulation, the bias measures the difference between the recorded and simulated motions averaged over all stations, and provides an indication of whether, on average, the simulation procedure is over-predicting, underpredicting, or even-predicting the recorded motions. The standard error measures the average difference between the simulated and recorded motions for a single observation, and provides an indication of the uncertainty involved in predicting a single value.

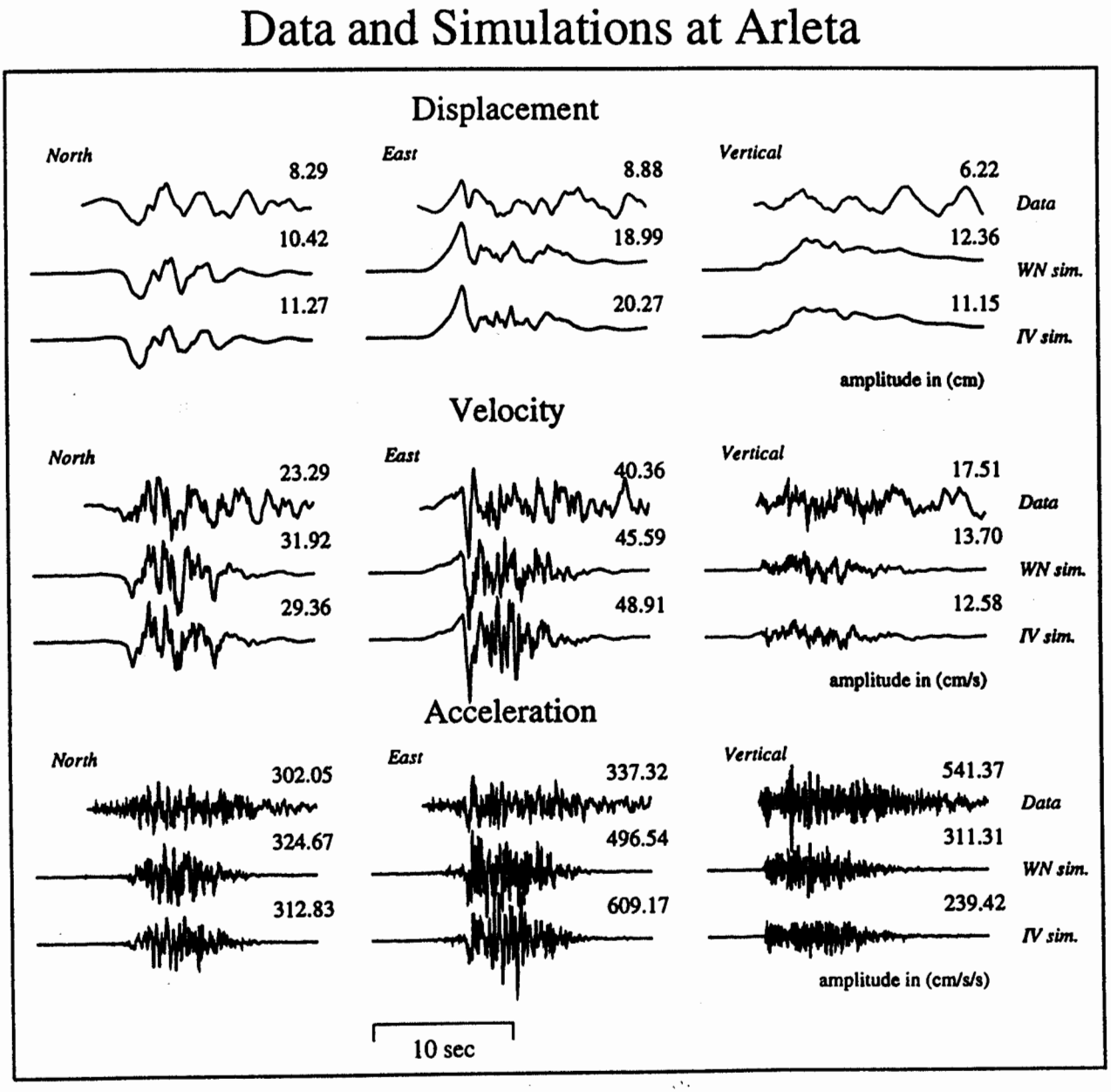

Figure 1-5. Comparison of recorded (top row) and simulated (middle and bottom rows) displacement, velocity and acceleration time histories at Arleta from the 1994 Northridge earthquake, plotted on a common scale, with peak value given in the top left corner.

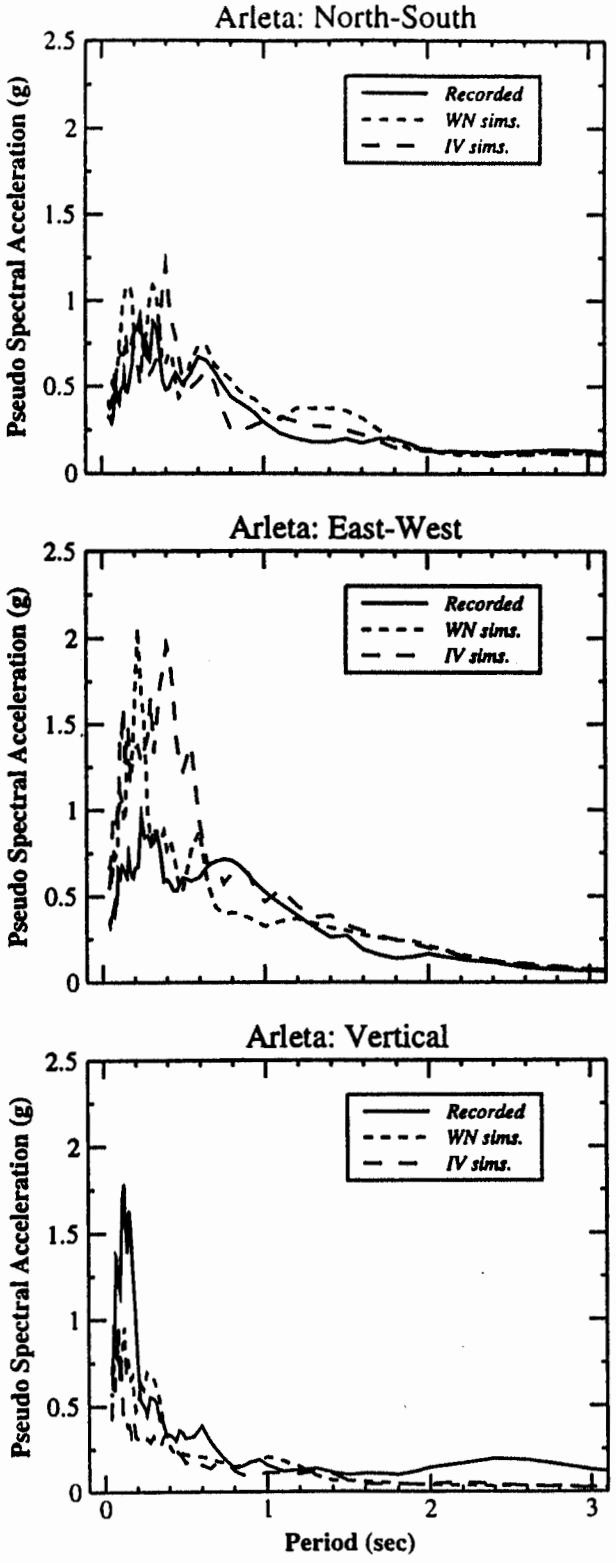

Figure 1-6. Comparison of recorded and simulated response spectra at Arleta.

As described in the following section, the deep geological structure had a significant effect on ground motions recorded in the Los Angeles basin during the Northridge earthquake. To avoid this complication, we concentrated our analysis on recordings of the Northridge earthquake in the San Fernando Valley. The goodness of fit in response spectral acceleration for recordings on soil sites in the San Fernando Valley, shown in the upper part of Figure 1-7, indicates that the simulation procedure predicts these motions with either no significant bias (i.e. within the 90% confidence intervals) or small bias in the period range of 0.2 to 35 Hz; there is a tendency for the long-period motions to be slightly underpredicted and the high frequency motions to be slightly overpredicted. This demonstrates that use of the Wald and Heaton (1994) rupture model of the Northridge earthquake, which was derived from the low frequency strong motion recordings, produces broadband ground motions whose engineering characteristics are compatible with the high frequency motions that were recorded during the earthquake.

In order to evaluate whether the ground motions recorded during the Northridge are representative of ground motions from thrust faults, or are anomalous due to an anomalous rupture model, we used the method described by Somerville et al. (1991a) to generate a suite of 20 rupture models that represent alternative realizations of rupture on the fault plane of the Northridge earthquake (Saikia and Somerville, 1995). The fit between the average response spectra derived from these 20 slip models and the response spectra recorded during the Northridge earthquake is shown in the lower part of Figure 1-7. The low bias indicates that the average value of the ground motions calculated using these 20 models is not significantly different from the data. We conclude that the large ground motions recorded during the Northridge earthquake and simulated using the Wald and Heaton (1994) rupture model are not attributable to an anomalous rupture model.

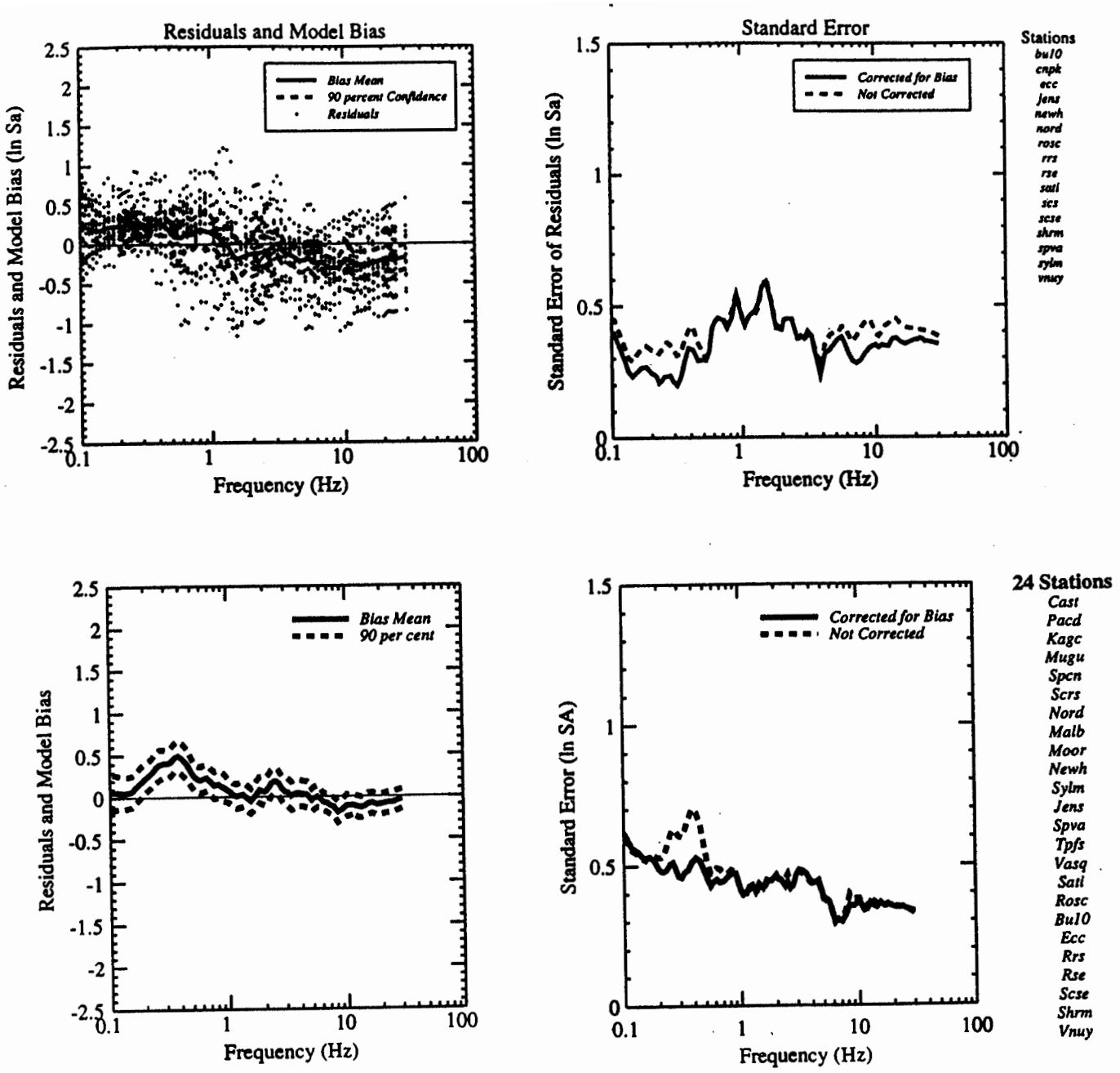

Figure 1-7. Top: Performance of the broadband simulations using the rupture model of Wald and Heaton (1994) in matching the 5% damped response spectra of the ground motions of the 1994 Northridge earthquake. Bottom: Comparison of the recorded response spectrum with the average response spectrum from 20 randomly generated rupture models representing alternative realizations of rupture on the fault plane of the Northridge earthquake. Figures on the left indicate the natural logarithm of model bias (positive bias indicates underprediction), and figures on the right indicate the natural logarithm of the standard error.

Response of the Los Angeles Basin during the Northridge Earthquake

The ground motions recorded in the Los Angeles Basin have larger amplitudes and longer durations than those recorded at comparable distances in other locations. The goodness of fit in response spectral acceleration for recordings on soil sites in the Los Angeles Basin (middle of Figure 1-8) indicates that the simulation procedure predicts these motions with no significant bias for frequencies larger than 0.5 Hz, but there is underprediction of the recorded motions for frequencies lower than 0.5 Hz by about a factor of 2. The long period ground motions recorded in the northwestern Los Angeles basin, especially in Santa Monica and West Los Angeles, are dominated by large, late arriving pulses. These are interpreted as surface waves generated by body waves that entered and became trapped within the southward-thickening margin of the Los Angeles basin (Graves, 1994). The trapping of waves in both large-scale (deep basin) and small-scale (local microbasin) structures (Saikia et al., 1994b) may explain the large motions recorded at distant isolated sites such as Santa Monica. Modifications of the motions simulated in the Los Angeles Basin to account for these effects, described by Somerville et al. (1995a), are quite effective at matching the amplitudes of the recorded data, as shown on the right side of Figure 1-8. The effects of large scale basin structure on the ground motions recorded in the San Fernando basin are less pronounced.

The ground motions recorded in the Los Angeles Basin also have longer durations than those recorded at comparable distances in other locations. Using the method of Husid (1969), we define duration as the time interval over which the integrated squared ground motion amplitude accumulates a specified fraction of its ultimate value (Husid, 1969). Because time histories tend to have small amounts of energy at the beginning and the end, we base the duration estimate on the time during which the cumulative energy increases from a low fraction such as 0.05 to a high fraction such as 0.75, and then prorate the measured duration using linear interpolation. In Figure 1- 9, we show examples of the fit of the duration of the recorded acceleration time histories to those of the simulated time histories as a function of the fraction of cumulative energy. The variable on the horizontal axis is the fraction of the total energy in the time history used as the upper limit in calculating the duration; the lower

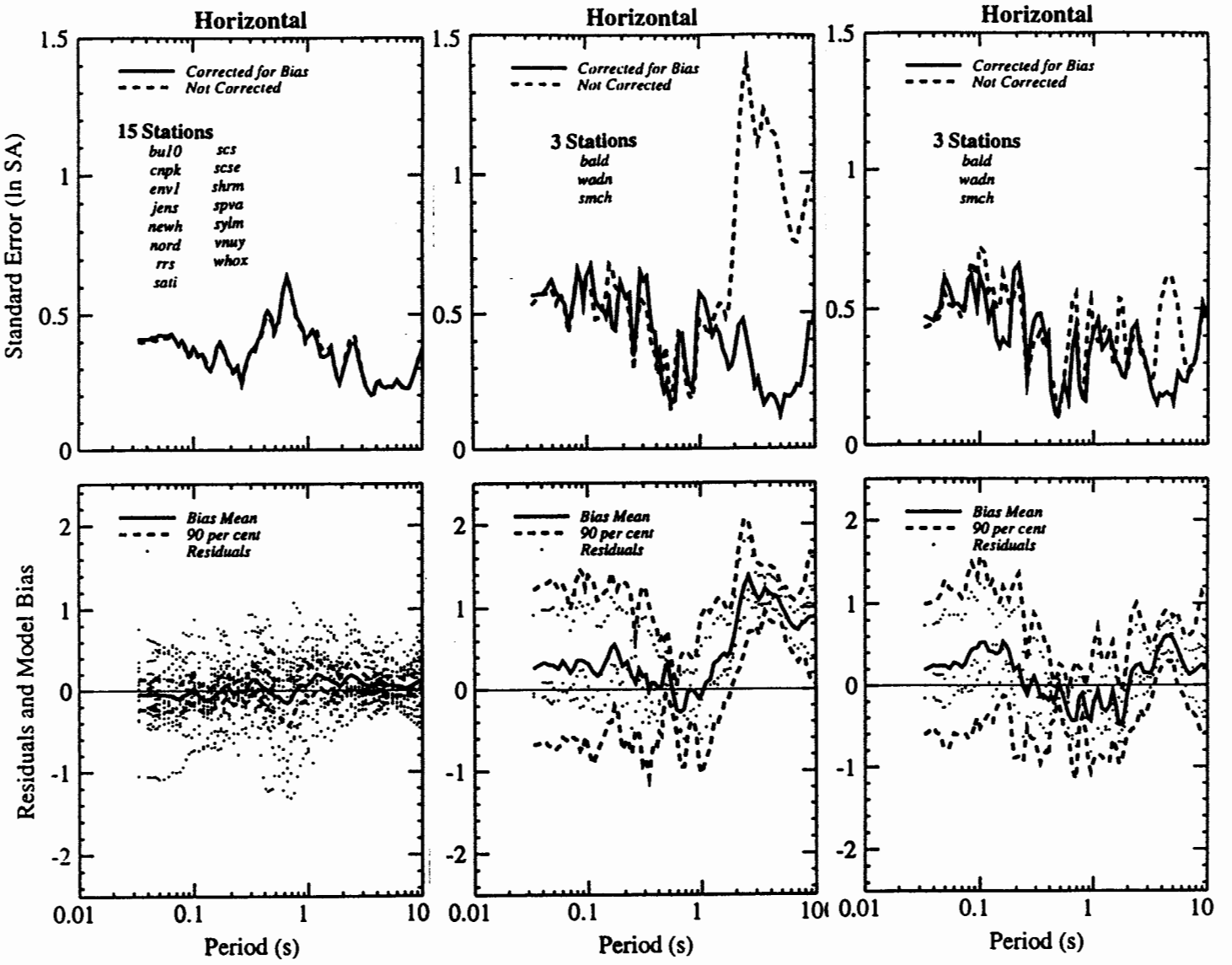

Figure 1-8. Performance of the broadband simulations using the rupture model of Wald and Heaton (1994) in matching the response spectra of the ground motions of the 1994 Northridge earthquake. Left: sites in the San Fernando Valley, which have little basin response. Center: sites in the Los Angeles Basin, which have significant basin response. Right: sites in the Los Angeles Basin, after modification of simulations to incorporate basin response following the procedure described by Somerville et al. (1995).

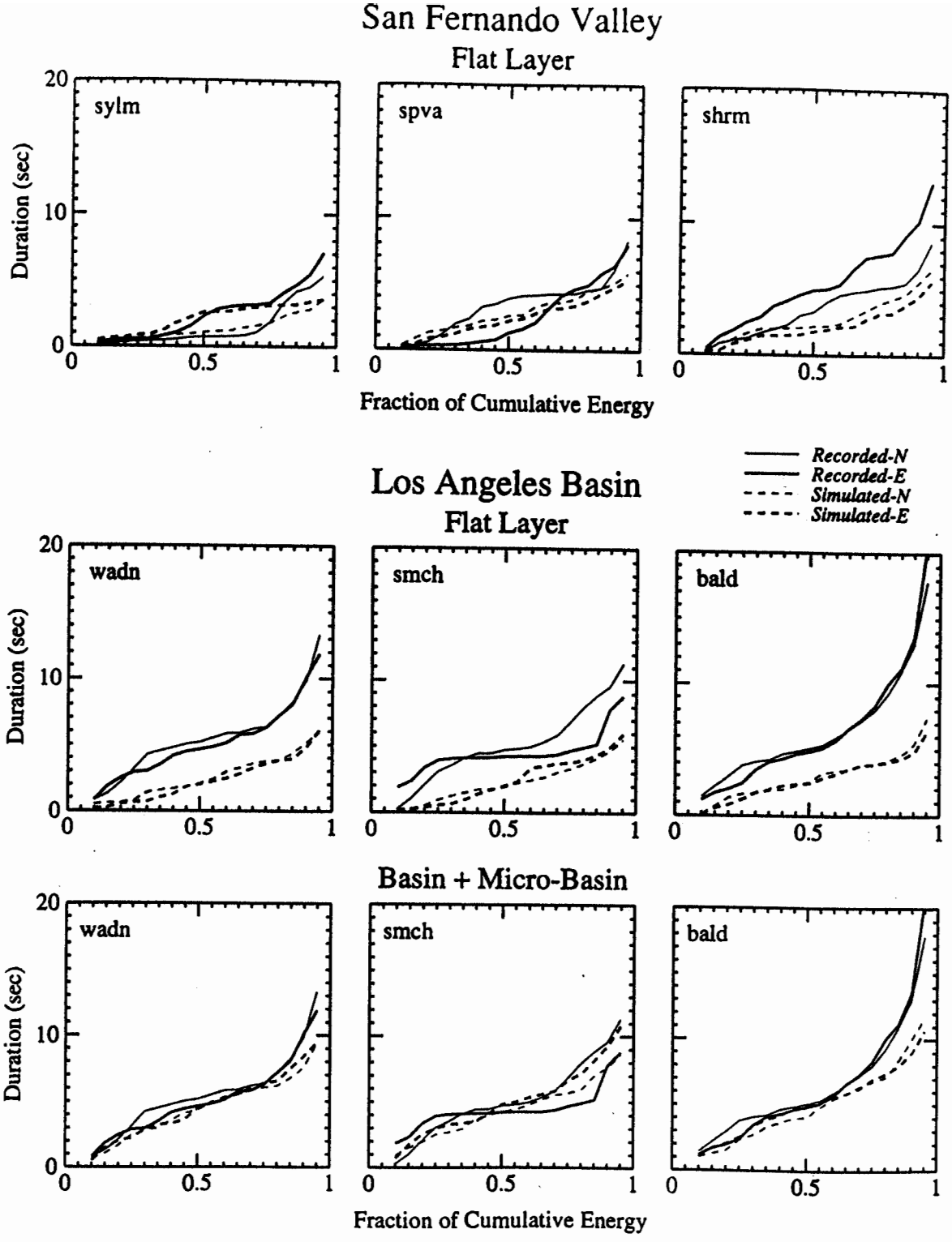

Figure 1-9. Performance of the broadband simulations using the rupture model of Wald and Heaton (1994) in matching the durations of the ground motions of the 1994 Northridge earthquake. Top: sites in the San Fernando Valley, which have little basin response. Center: sites in the Los Angeles Basin, which have significant basin response. Bottom: sites in the Los Angeles Basin, after modification of simulations to incorporate basin response following the procedure described by Somerville et al. (1995).

limit is set at 0.05. Generally, the agreement is fairly good for the San Fernando Valley sites, shown in the upper row, with the recorded duration about 60% larger on average than the simulated duration. The misfit between recorded durations and those simulated using the 1-D geologic model is much more severe in the Los Angeles Basin than in the San Fernando Valley, as shown in the center row; the recorded durations are about 100% longer. Modification of the simulated time histories in the Los Angeles Basin to take account of basin effects, described by Somerville et al. (1995a), produces good agreement, as shown in the lower row.

Implication of the Northridge Strong Motions for Empirical Attenuation Relations for Earthquakes on Thrust Faults

The peak accelerations from the Northridge earthquake were about 50% larger (about one standard deviation larger) than the median value predicted by current empirical attenuation relations at distances less than about 30 km, as shown in Figure 1-1a. This raises the question of whether the ground motions resulting from the Northridge earthquake are anomalous for thrust events, or are representative of the ground motions expected in future thrust earthquakes. The empirical data base contains few strong motion records close to large thrust earthquakes, making it difficult to assess whether the Northridge ground motions are anomalous based on recorded data alone. Accordingly, we have used results from our broadband strong motion simulation procedure to augment the existing data base and help assess whether the ground motions from this event were anomalous.

Based on the rupture model of Wald and Heaton (1994), the source characteristics and rupture process of the Northridge earthquake do not appear to be anomalous when compared with those of other crustal earthquakes (Wald, 1992; Somerville and Abrahamson, 1991; Somerville et al., 1991). In particular, the relationship between fault rupture area (about 400 km^2) and seismic moment (about 1.2×10^{26} dyne.cm), which is a measure of the static stress drop of the earthquake, is compatible with that of other crustal earthquakes. Also, asperites (defined as regions where the slip is larger than the slip averaged over the entire rupture area) make up about 25% of the rupture area, compatible with the average value of 26% derived

from other crustal earthquakes in California.

The ground motions from the Northridge earthquake and our simulations of these ground motions have a similar pattern of departure from empirical attenuation relations for thust earthquakes: the peak accelerations are at about the 84th percentile level for distances within 20 to 30 km, and follow the median level for larger distances, as shown in Figure 1-1a and 1-1c. The same pattern of departure from empirical attenuation relations was obtained in our pre-Northridge simulations of the peak accelerations of an Elysian Park blind thrust event (Figure 1-1b). The fact that we are able to model this pattern with broadband simulations, and had done so before the Northridge earthquake occurred, suggests that the recorded Northridge motions are not anomalous.

Based on our modeling of the strong ground motions recorded during the Northridge earthquake, it appears that the Northridge strong motion records are not anomalous but are representative of ground motions close to thrust faults. Accordingly, it seems appropriate to include these recordings in strong motion data sets that are used to develop empirical ground motion attenuation relations, and to use these augmented data sets as the basis for evaluating the need for modifications in design coefficients in the seismic provisions of building codes.

CHAPTER 2. EMPIRICAL ANALYSIS OF THE EFFECT OF THE HANGING WALL AND FOOT WALL ON GROUND MOTIONS

Introduction

Recent empirical attenuation relation studies have generally found that peak horizontal accelerations from thrust earthquakes are 20-30% larger than from strike-slip earthquakes for the same magnitude and closest distance (e.g. Campbell 1993; Idriss 1991; Sadigh et al, 1993; Boore et al., 1994). This effect of earthquake mechanism on the ground motion has been called the style-of-faulting factor. For most attenuation relations, the style-of-faulting factor is simply a scale factor that is applied at all magnitudes and distances, and often the style-of-faulting factor derived for peak acceleration is assumed to apply to response spectral values at all periods as well.

A recent study by Campbell and Bozorgnia (1994) examined the distance and magnitude dependence of the style-of-faulting factor. They found that the style-of-faulting factor decreased with increasing magnitude and distance, but they did not distinguish between sites on the hanging wall from those on the foot wall. Hanging wall and foot wall are geological terms coined by miners that refer to the upper and lower sides respectively of dipping faults. In this study, we have used a modified definition of hanging wall and foot wall which is defined in Figure 2-1.

Thrust earthquakes typically occur on non-vertically dipping faults. For dipping faults, the ground motion is not expected to be the same on both sides of the fault. Based on simple geometry alone, we expect that sites located above the fault rupture on the hanging wall will have larger ground motions than sites at the same rupture distance located on the foot wall because the hanging wall sites are closer to a larger area of the source than the foot wall sites (Figure 2-1). This difference in the proximity of the source to the site is a result of using the shortest distance to the rupture plane as the definition of the closest distance.

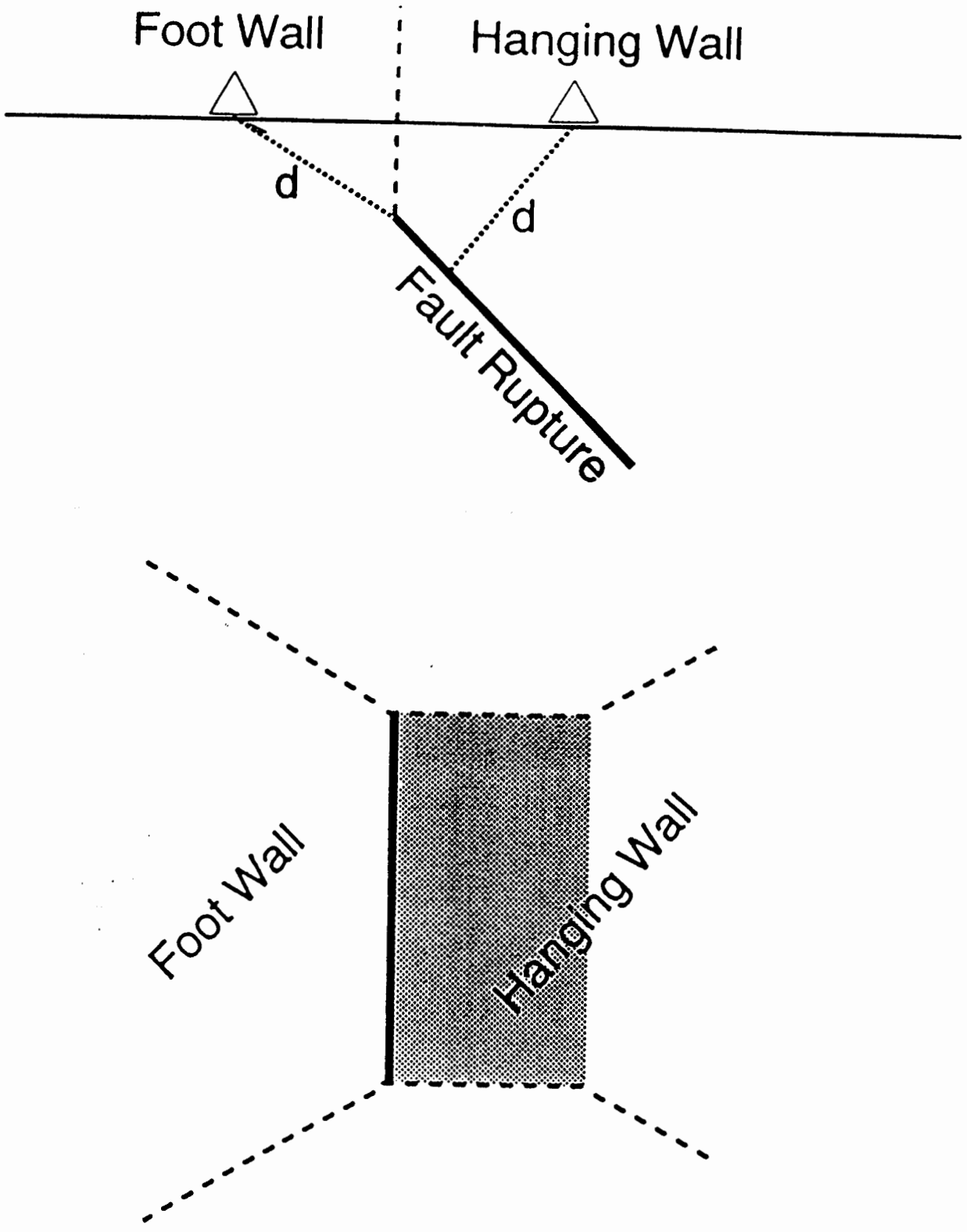

Figure 2-1. Definition of foot wall and hanging wall sites used in this analysis. The separation point is the vertical projection of the top of the rupture, as shown in the vertical cross section (upper frame). Stations off the ends of the fault are excluded, as shown in the map view (lower frame).

For fault ruptures that do not reach the surface, we define the separation between the hanging wall and foot wall by the vertical projection of the top of the rupture plane (Figure 2-1). Using this definition, the hanging wall and foot wall motions must become equal for sites located directly over the top edge of the fault. Therefore, it does not make sense to simply estimate separate hanging wall and foot wall style-of-faulting factors. To do so would create a discontinuity at the surface projection of the top of the rupture. An alternative to the definition of the hanging wall and foot wall sites for buried faults would be based on projecting up the dip of the fault to the surface rather than using a vertical projection. Since we think that the main difference in high frequency motions on the hanging wall and foot wall are due to the proximity differences, this alternative definition would not be appropriate.

In this study, we examine the ground motions from the 1994 Northridge earthquake and other reverse and reverse/oblique events to determine the systematic differences in the ground motion recorded on the hanging wall and foot wall. Sites off the edge of the fault rupture are excluded from the hanging wall and foot wall effects (Figure 2-1).

Approach

The effect of the hanging wall and foot wall on strong ground motions is evaluated by examining the residuals of the ground motion from attenuation relations. Since the Northridge earthquake was so well recorded, we first evaluate the hanging wall effects from the Northridge earthquake and then later evaluate the average hanging wall effect for a larger data set. For the Northridge evaluation, Northridge specific attenuation relations are developed using all available strong motion recordings (including stations off the ends of the fault) and then the residuals from stations on the hanging wall and foot wall are examined to quantify the systematic differences in the ground motions on the two sides of the fault. For the larger data set, average attenuation relations are developed and the same functional form that was used to model the hanging wall effect during the Northridge earthquake is included as part of the regression equation.

Data Set

For the Northridge event, the available strong motion recordings from CSMIP, DWP, USGS, and USC with rupture distances less than 200 km were considered in this analysis. To avoid potentially significant structure effects on the recorded ground motions, recordings from buildings that are greater than two stories in height were excluded from the data set. In addition, recordings from abutments of dams were also excluded. The Geomatrix site classification scheme (Table 2-1) was used for this study with classes A and B considered as "rock" and classes C and D considered as "soil". Recordings on soft soil (class E) were excluded. The resulting data set consists of 196 stations of which 151 were available in digital from at the time of this study. For all of the ground motion parameters used in this study, the geom
etric average of the ground motion on the two horizontal components is used. The stations on the footwall and hanging wall are listed in Table 2-2.

The closest distance to the rupture plane was computed for each station based on the slip model of Wald and Heaton (1994). The surface projection of the rupture plane and nearby recording stations are shown in Figure 2-2. The irregular model of the rupture plane takes into account the low slip in the north east corner.

For the analysis of the larger data set, the strong motion data set used by Abrahamson and Silva (1995) is used. This data set includes soil and rock recordings out to 200 km from the 50 events listed in Table 2-3.

Regression Models

To examine the differences in the ground motion on the hanging wall and foot wall, we need to remove the average effects of the attenuation. The large number of recordings from the Northridge earthquake makes it possible to develop a Northridge-specific attenuation model rather than using a generic attenuation relation. Since the objective of the regression

Table 2-1. Site Classification Scheme (From Geomatrix Consultants)

A Rock

Instument is founded on rock material (Vs > 600 mps or a very thin veneer (less than 5m) of soil overlying rock material.

B Shallow (stiff) soil

Instrument is founded in/on a soil profile up to 20 m thick overlying rock material

C Deep narrow soil

Instrument is founded in/on a soil profile at least 20 m thick overlying rock material in a narrow canyon or valley no more than several km wide

D Deep broad soil

Instrument is founded in/on a soil profile at least 20 m thick overlying rocl material in a broad canyon or valley

E Soft deep soil

Instrument is founded in/on a deep soil profile that exhibits low average shear wave velocity (Vs < 150 m/s)

Table 2-2. Footwall and Hanging wall stations for the Northridge Data Set

Code	Station Name	Org.	Site	Loc
pacd	Pacoima Dam Downstream	CSMIP	Rock	FW
vasq	Vasquez Rock Park	CSMIP	Rock	FW
lh04	Lake Hughes #4	CSMIP	Rock	FW
lh09	Lake Hughes #9	CSMIP	Rock	FW
sylm	Sylmar - Olive View Parking Lot	CSMIP	Soil	FW
cnyn	16629 Lost Cyn Rd	USC	Soil	FW
newh	Newhall, LA Co Fire Sta	CSMIP	Soil	FW
eliz	Elizabeth Lake	CSMIP	Soil	FW
lh12	Lake Hughes #12	CSMIP	Soil	FW
nido	Monte Nido Fire Sta	USGS	Rock	HW
malb	Malibu - Point Dume	CSMIP	Rock	HW
scse	Sylmar Conv Sta E free-field	DWP	Soil	HW
jens	Jensen Filtration Plant - Adm Bld	USGS	Soil	HW
spva	Sepulveda VA Hospital - grnd	USGS	Soil	HW
sati	17645 Saticoy St, Northridge	USC	Soil	HW
cnpk	Canoga Park, Topanga Cyn Blvd	USC	Soil	HW
svsc	Simi Valley, 6334 Katherine	USC	Soil	HW
ssus	Santa Susana, free-field	USGS	Soil	HW
tarz	Tarzana	CSMIP	Soil	HW
tpfs	Topanga Fire Sta	USGS	Soil	HW
ppsb	Pacific Palisades Fire Sta	USC	Soil	HW
rrs	Rinaldi Receiving Sta FF	DWP	Soil	HW

Table 2-3. Earthquakes in the expanded data set

Event #	Earthquake	Date & Time	Mag
6	Imperial Valley	1940 0519 0437	6.9
12	Kern County	1952 0721 1153	7.4
20	San Francisco	1957 0322 1944	5.3
25	Parkfield	1966 0628 0426	6.1
28	Borrego Mtn	1968 0409 0230	6.8
29	Lytle Creek	1970 0912 1430	5.4
30	San Fernando	1971 0209 1400	6.6
31	Point Mugu	1973 0221 1445	5.8
32	Hollister	1974 1128 2301	5.2
34	Oroville	1975 0801 2020	5.9
35	Oroville	1975 0802 2022	5.1
36	Oroville	1975 0802 2059	4.4
37	Oroville	1975 0808 0700	4.7
39	Gazli, USSR	1976 0517	6.8
42	Santa Barbara	1978 0813	6.0
43	Tabas, Iran	1978 0916	7.4
44	Coyote Lake	1979 0806 1705	5.7
45	Imperial Valley	1979 1015 2316	6.5
46	Imperial Valley	1979 1015 2319	5.2
47	Imperial Valley	1979 1016 0658	5.5
48	Livermore	1980 0124 1900	5.8
49	Livermore	1980 0127 0233	5.4
50	Anza	1980 0225 1047	4.9
59	Victoria, Mexico	1980 0609 0328	6.4
63	Westmorland	1981 0426 1209	5.8
66	Coalinga	1983 0502 2342	6.4
67	Coalinga	1983 0509 0249	5.0
68	Coalinga	1983 0611 0309	5.3
69	Coalinga	1983 0709 0740	5.2
70	Coalinga	1983 0722 0239	5.8
71	Coalinga	1983 0722 0343	4.9
72	Coalinga	1983 0725 2231	5.2
74	Coalinga	1983 0909 0916	5.3
76	Morgan Hill	1984 0424 2115	6.2
77	Bishop (Rnd Val)	1984 1123 1912	5.8
79	Nahanni, Canada	1985 1223	6.8
80	Hollister	1986 0126 1920	5.4
83	N. Palm Springs	1986 0708 0920	6.1
84	Chalfant Valley	1986 0720 1429	5.9
85	Chalfant Valley	1986 0721 1442	6.2
86	Chalfant Valley	1986 0721 1451	5.6
87	Chalfant Valley	1986 0731 0722	5.8
89	Whittier Narrows	1987 1001 1442	6.0
90	Whittier Narrows	1987 1004 1059	5.3
91	Superstitn Hills(A)	1987 1124 0514	6.3
92	Superstitn Hills(B)	1987 1124 1316	6.7
94	Loma Prieta	1989 1018 0005	6.9
96	Cape Mendocino	1992 0425 1806	7.1
97	Landers	1992 0628 1158	7.3
98	Northridge	1994 0117 1231	6.7

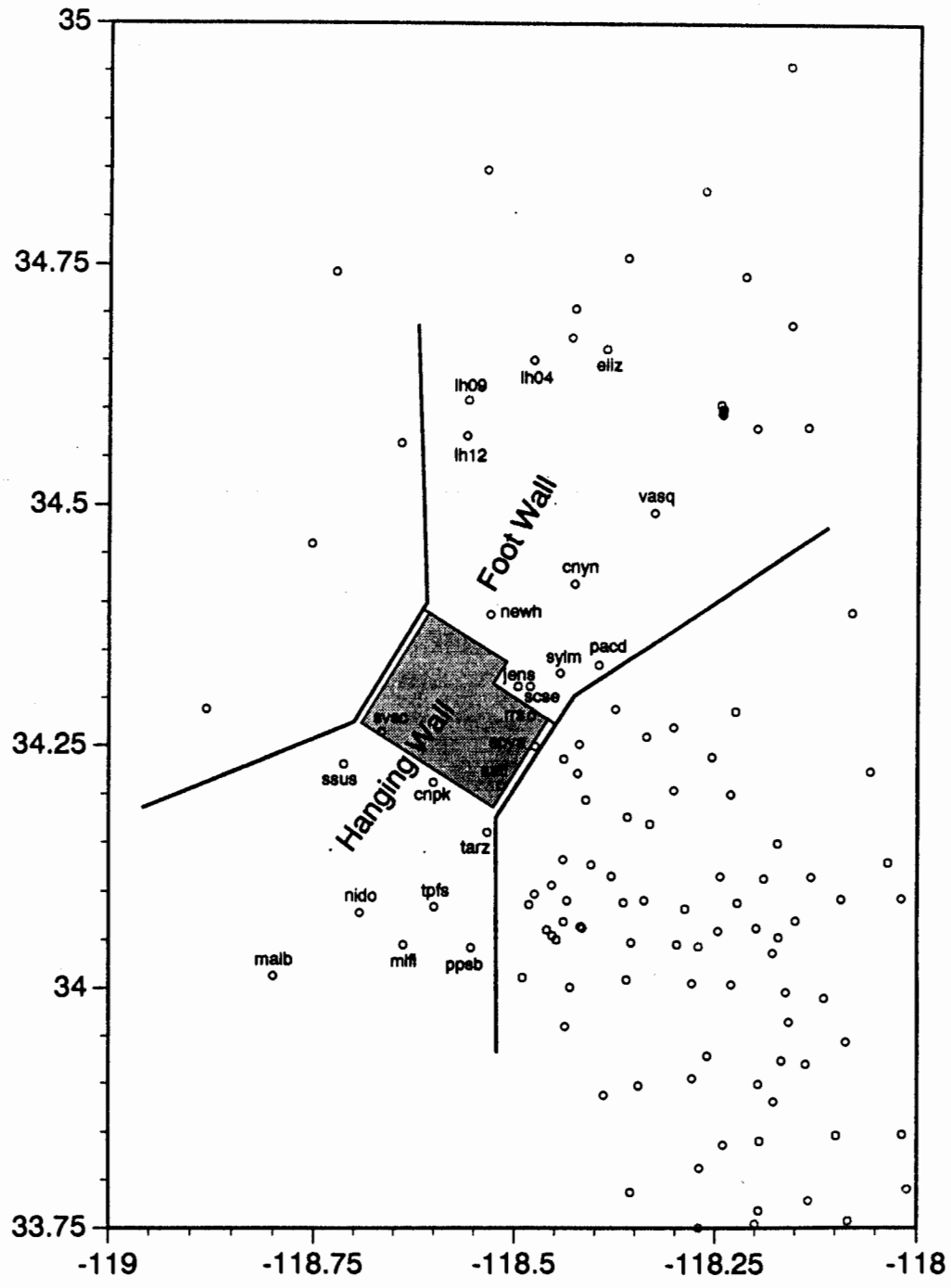

Figure 2-2. Nearby recordings stations from the Northridge Earthquake used in this paper. The surface projection of the rupture plane from Wald and Heaton (1994) is shown by the shaded region.

model is to remove the average attenuation effects, we have used a simple form of the attenuation relation. The reference ground motion attenuation relation for the Northridge earthquake is modeled using the following functional form for the natural logarithm of spectral acceleration:

$$ln\ Y(g) = a_1 + a_2 S + (b_1 + b_2 S)\ ln\ (r+c)\ , \quad (1)$$

where Y is the spectral acceleration in g, r is the rupture distance in km, and S is a site flag which is 0 for rock sites and 1 for soil sites.

The coefficients for peak acceleration estimated using ordinary least-squares are listed in Table 2-4. The resulting peak acceleration attenuation relations for rock and soil sites are shown with the data in Figure 2-3. The residuals of this fit, defined as the natural log of the data minus the natural log of the value predicted by the model, are shown separately for rock and soil sites in Figures 2-4a and 2-4b, respectively. The spectral acceleration at 5% damping was computed using the Nigam and Jennings (1969) algorithm for all of the recordings with digital accelerograms available. The results of the regression analysis for the spectral values are also given in Table 2-4.

Hanging Wall and Foot Wall Effects

The hanging wall and foot wall effects are evaluated by examining the residuals from the Northridge specific attenuation relations. Figure 2-5 shows the peak acceleration residuals for sites on the hanging wall and foot wall. In this figure, the footwall sites are plotted at negative distances to separate them from the hanging wall sites. The peak acceleration residuals on the hanging wall appear to be biased to positive values for the distance range of 8 to 30 km (e.g. the attenuation model under predicts these peak accelerations) whereas the residuals for foot wall sites do not show a significant bias over this distance range. The mean bias of the 10 hanging wall sites at distances of 8 to 30 km is 0.29 $\pm$ 0.15. While suggestive of a difference in the hanging wall and foot wall motions, the Northridge data by themselves are not conclusive due to the small numbers of recordings on the hanging wall.

Table 2-4. Coefficients for Northridge-Specific Attenuation Relation

period	a_1	a_2	b_1	b_2	c	s
0.0	3.214	-0.519	-1.404	0.170	6.3	0.44
0.2	4.408	-1.369	1.637	-0.333	22.4	0.48
0.3	3.070	-1.100	1.181	-0.245	11.2	0.49
0.5	3.453	-1.289	0.499	-0.042	9.9	0.49
1.0	1.251	-0.988	0.939	-0.152	0.6	0.46
2.0	-0.100	-0.953	1.251	-0.158	0	0.50
4.0	-0.929	-1.025	0.933	-0.098	0	0.52

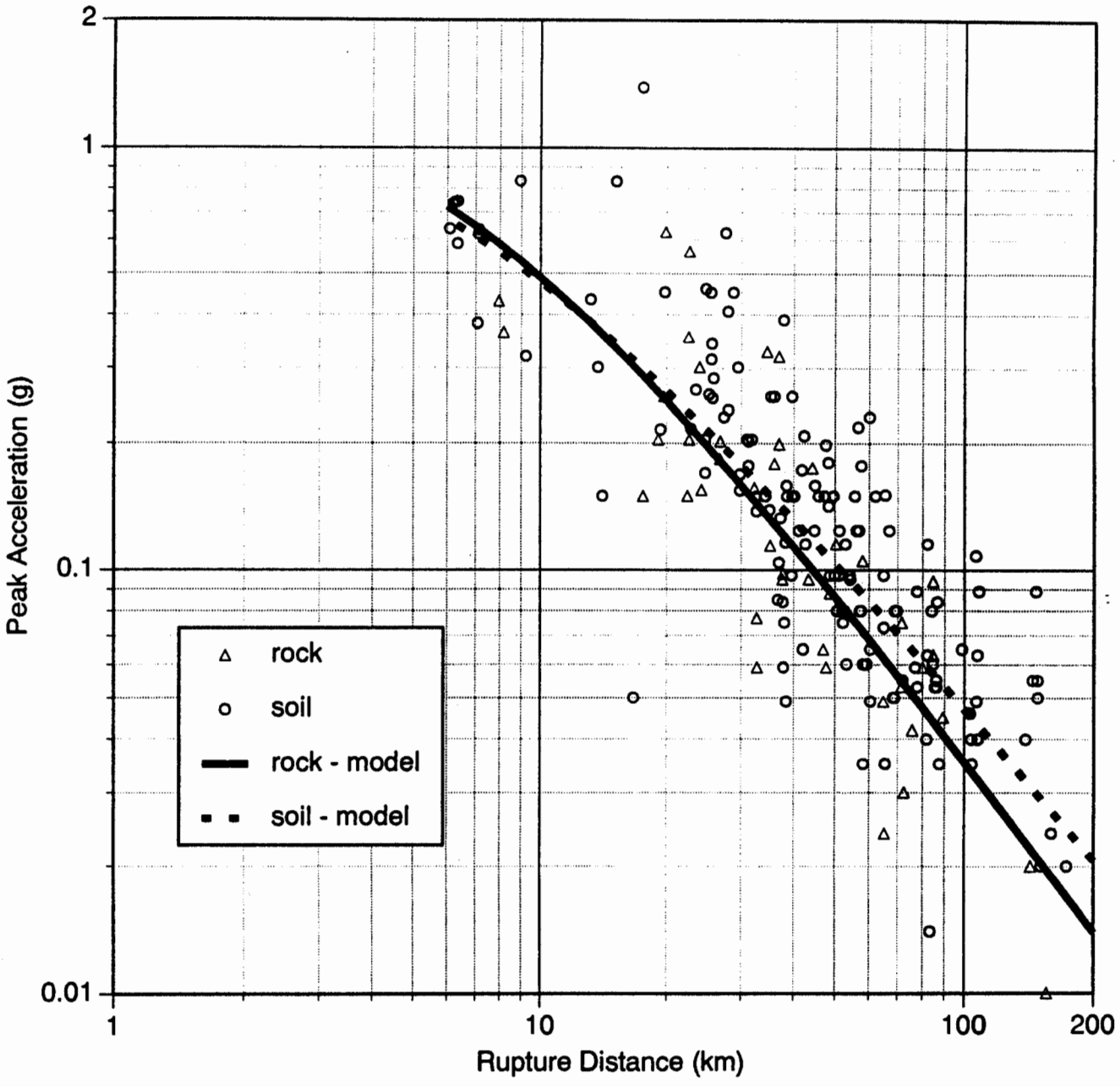

Figure 2-3. Northridge-specific attenuation relation for peak acceleration.

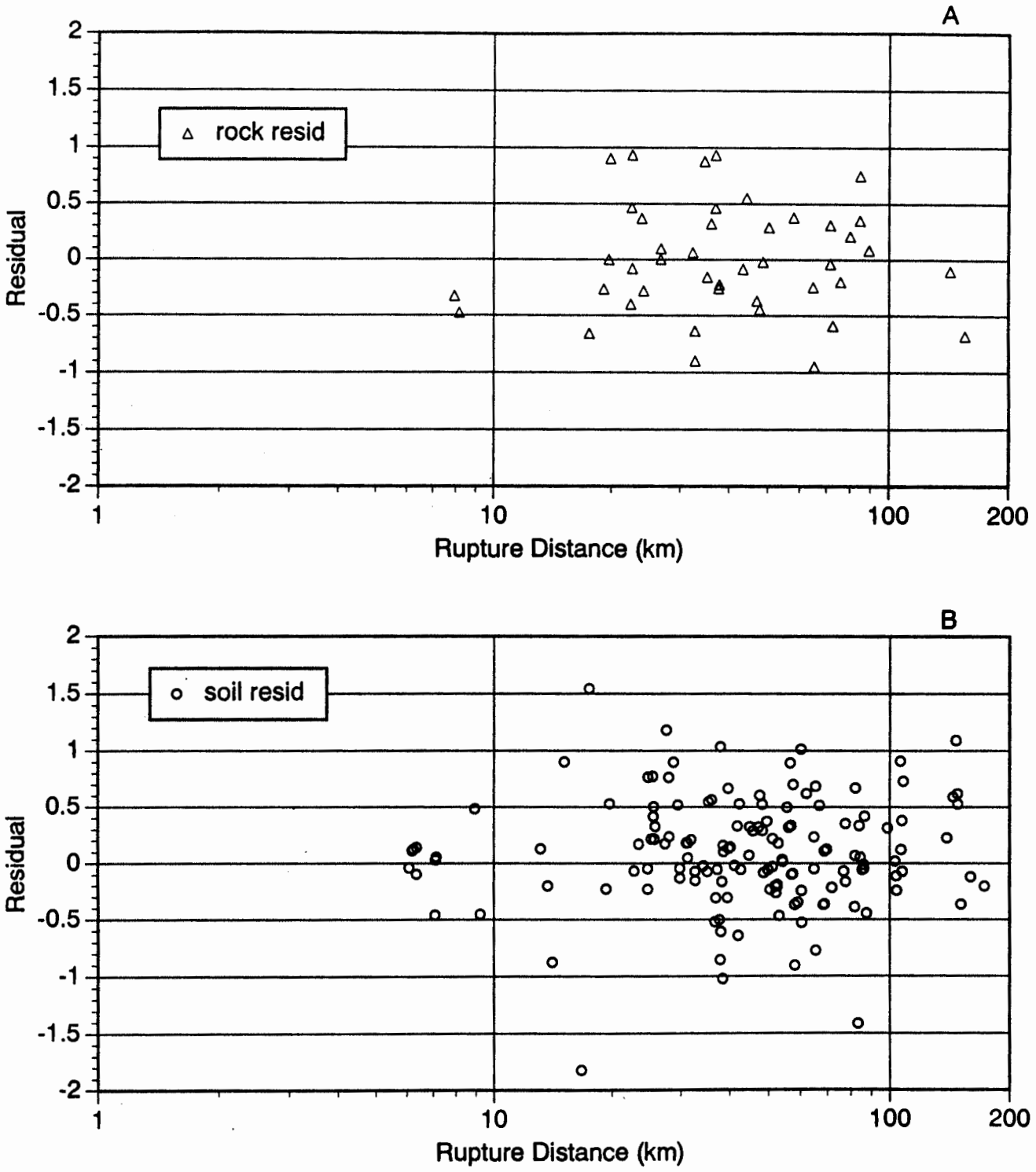

Figure 2-4. Residuals of peak horizontal acceleration from the reference model. (A) Rock sites. (B) Soil sites.

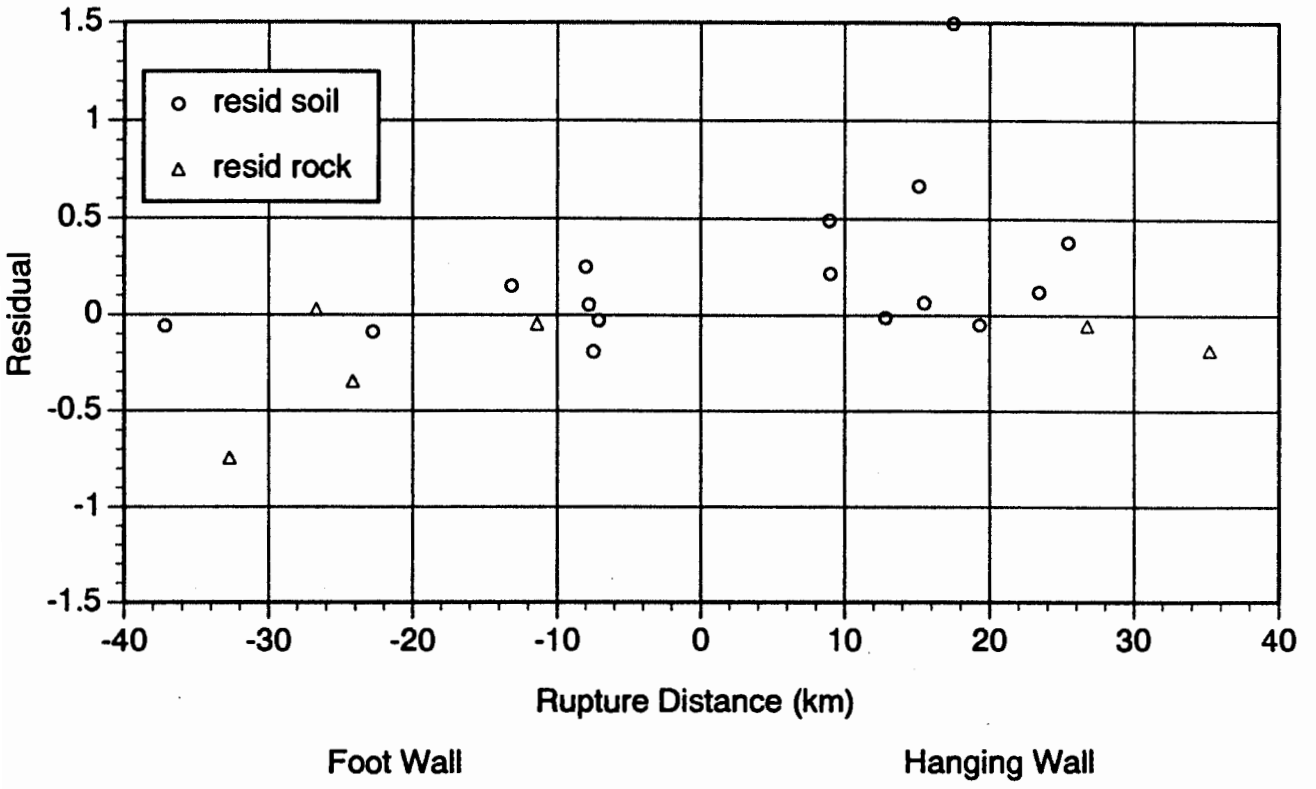

Figure 2-5. Residuals of peak acceleration for sites on the hanging wall (plotted as positive distances) and foot wall (plotted as negative distances).

However, if we consider ground motions from other dipping faults, the effect becomes more obvious. Abrahamson and Somerville (1993) examined recordings from other reverse events to estimate the distance dependence of the style-of-faulting factor for peak horizontal acceleration including the distinction between hanging wall and foot wall. They used empirical recordings from 11 reverse-oblique and reverse events with $M \geq 6.0$ (Table 2-5). The residuals of the oblique and reverse event peak accelerations were computed from the Sadigh et al. (1993) and Sadigh (1987) attenuation relations for rock and soil, respectively and are shown in Figure 2-6. The residuals from the Northridge earthquake are also shown in this figure. The trend of the residuals from the other earthquakes is consistent with the Northridge data. The mean residual on the hanging wall for distances of 5-20 km is 0.43 ± 0.09 and on the foot wall the mean residual over this distance range is -0.24 ± 0.10. Thus the difference in the mean residual on the hanging wall and footwall over this distance range is 0.67 ± 0.14.

In addition, Abrahamson and Somerville (1993) also showed that the same trend can be found using numerical simulations for dipping faults. A similar result has been found from other numerical modeling studies (Walt Silva, personal communication). In light of these other data, the increase in peak accelerations on the hanging wall observed during the Northridge earthquake is likely to be a systematic effect that can be expected for future reverse and reverse/oblique events.

Table 2-5. Other Events Used Analysis of Hanging Wall / Foot Wall Effects

				Number of Recordings	
Event	**M**	**Dip**	**Mech**	**Foot**	**Hang**
1952 Kern County	7.4	67	RV	1	0
1971 San Fernando	6.6	53	RV	3	1
1976 Gazli	6.8	38	RV	0	1
1978 Santa Barabara	6.0	30	RV	0	1
1978 Tabas	7.4	30	RV	1	2
1983 Coalinga	6.5	32	RV	0	2
1985 Nahanni	6.8	23	RV	1	2
1986 N. Palm Springs	6.0	41	OBL	2	5
1989 Loma Prieta	7.0	70	OBL	6	3
1992 Cape Mendocino	7.1	13	RV	0	3
Total				14	20

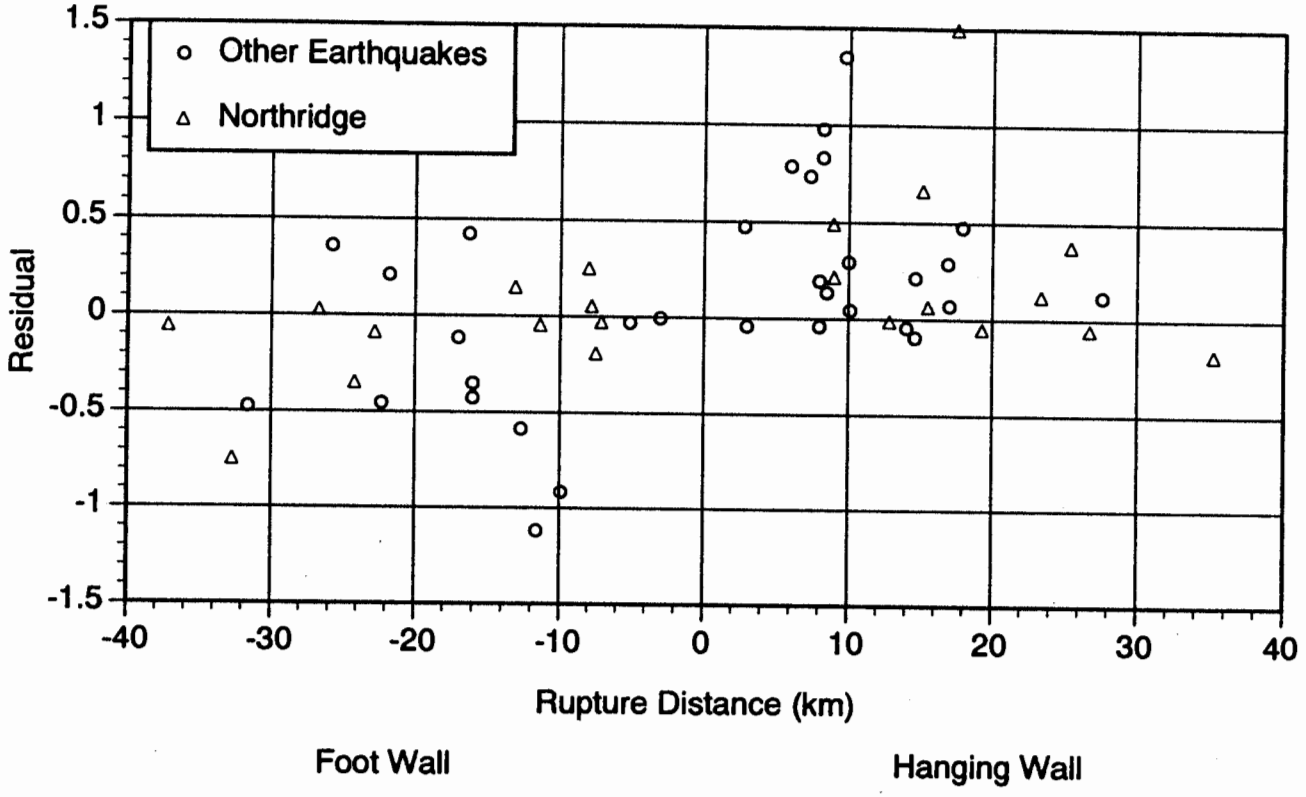

Figure 2-6. Comparison of hanging wall and foot wall effects on peak horizontal acceleration residuals from the Northridge Earthquake with that from other reverse and reverse/oblique events.

Model of Hanging Wall Effects

Based on the trends in the residuals (Figure 2-5), the following piece wise continuous functional form is used for the distance dependence of the peak acceleration residuals on the hanging wall during the Northridge earthquake:

$$\phi_{HW}(r) = \begin{cases} 0 & for\ 0 \le r \le x_1 \\ \frac{c}{2}\left[\cos\left(\frac{\pi(r-x_1)}{x_2-x_2}+\pi\right)+1\right] & for\ x_1 < r < x_2 \\ c & for\ x_2 \le r \le x_3 \\ \frac{c}{2}\left[\cos\left(\frac{\pi(r-x_3)}{x_4-x_3}\right)+1\right] & for\ x_3 < r < x_4 \\ 0 & for\ r \ge x_4 \end{cases} \quad (3)$$

where $\phi_{HW}(r)$ is the hanging wall effect. The boundary distances, x_1, x_2, x_3, and x_4 were first estimated using ordinary least-squares for the data with the additional earthquakes; there are too few Northridge data to determine these parameters. For Northridge, the minimum distance is 6 km due to the depth of the top of the rupture. Therefore, x_1 was fixed at 6 km. With the x_1, x_2, x_3, and x_4 values fixed, the constant c was estimated for the Northridge data set by itself using ordinary least-squares. The resulting parameter values are listed in Table 2-6 and the model is plotted in Figure 2-7. The results of the regression show that for sites located at closest distances of 10 to 20 km, the hanging wall model resulting in an increase of about 50% compared to the median attenuation for Northridge.

Table 2-6. Coefficients for Northridge Hanging Wall Effects on Peak Horizontal Acceleration

Parameter	Value
x_1	2
x_2	8
x_3	20
x_4	30
c	0.41

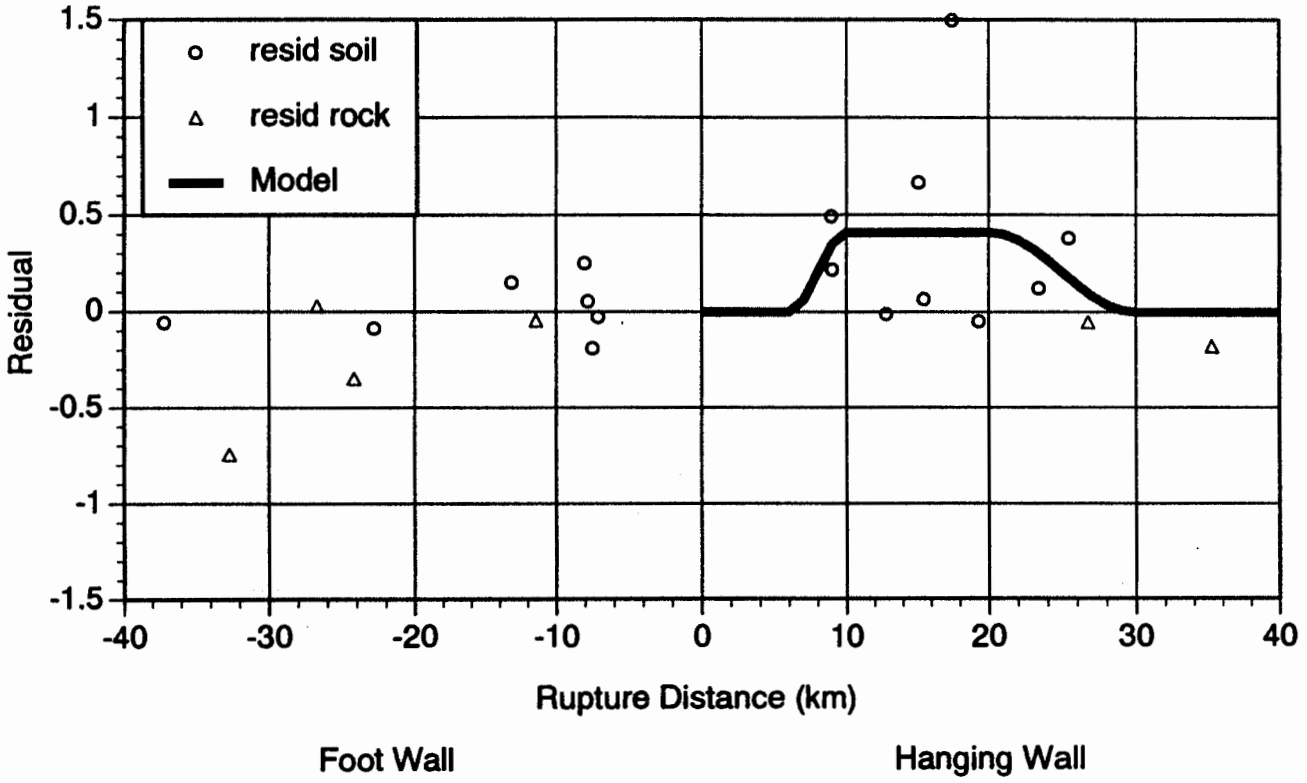

Figure 2-7. Regression model of the peak acceleration residuals on the hanging wall and foot wall.

Results for Response Spectral Values

The hanging wall / foot wall effect was also evaluated for several response spectral periods. Plots of the residuals for the spectral acceleration at periods of 0.2 to 4.0 seconds are shown in Figure 2-8. At periods of 0.2 to 0.3 seconds, the trend of the residuals is consistent with the peak acceleration residuals. At periods of 1.0 to 4.0 seconds, there is a change in the trends of the residuals on the hanging wall: the hanging wall residuals at 15-25 km are reduced. We interpret this effect to be due to directivity. For rupture up-dip, sites on both the hanging wall and foot wall close to the top edge of the rupture will experience strong directivity effects which result in increased long period motion.

As described by Somerville and Graves (1993) and Somerville et al. (1995b), rupture directivity effects increase the long period ground motion on the component normal to the fault strike relative to the ground motion on the component parallel to the fault strike because the near-fault fault parallel motion is nearly nodal due to radiation pattern effects, whereas the fault-normal component is near a radiation pattern maximum near the fault. Rupture directivity effects are largest in the region centered on the updip projection of the rupture surface. By our definition of foot wall and hanging wall, this region occupies more of the foot wall than the hanging wall. For the fault-normal peak velocity, the effect of rupture directivity on the foot wall increases the ground motions and causes them to be as large as on the hanging wall, counteracting the tendency for the proximity effect to make the hanging wall motion larger.

Analysis of the Larger Data Set

Using the larger data set from Abrahamson and Silva (1997), the effect of the hanging wall is evaluated for response spectral values for both the horizontal and vertical components. The same functional form as was developed for the Northridge event (Eq. 3) is used with values of x1, x2, x3, and x4 were estimated to be 4, 8, 18, and 25 km respectively. The resulting estimates of the maximum effect (coefficient c in Eq 3) are shown in Figure 2-9 as functions of period for the horizontal and vertical components. The standard errors of the

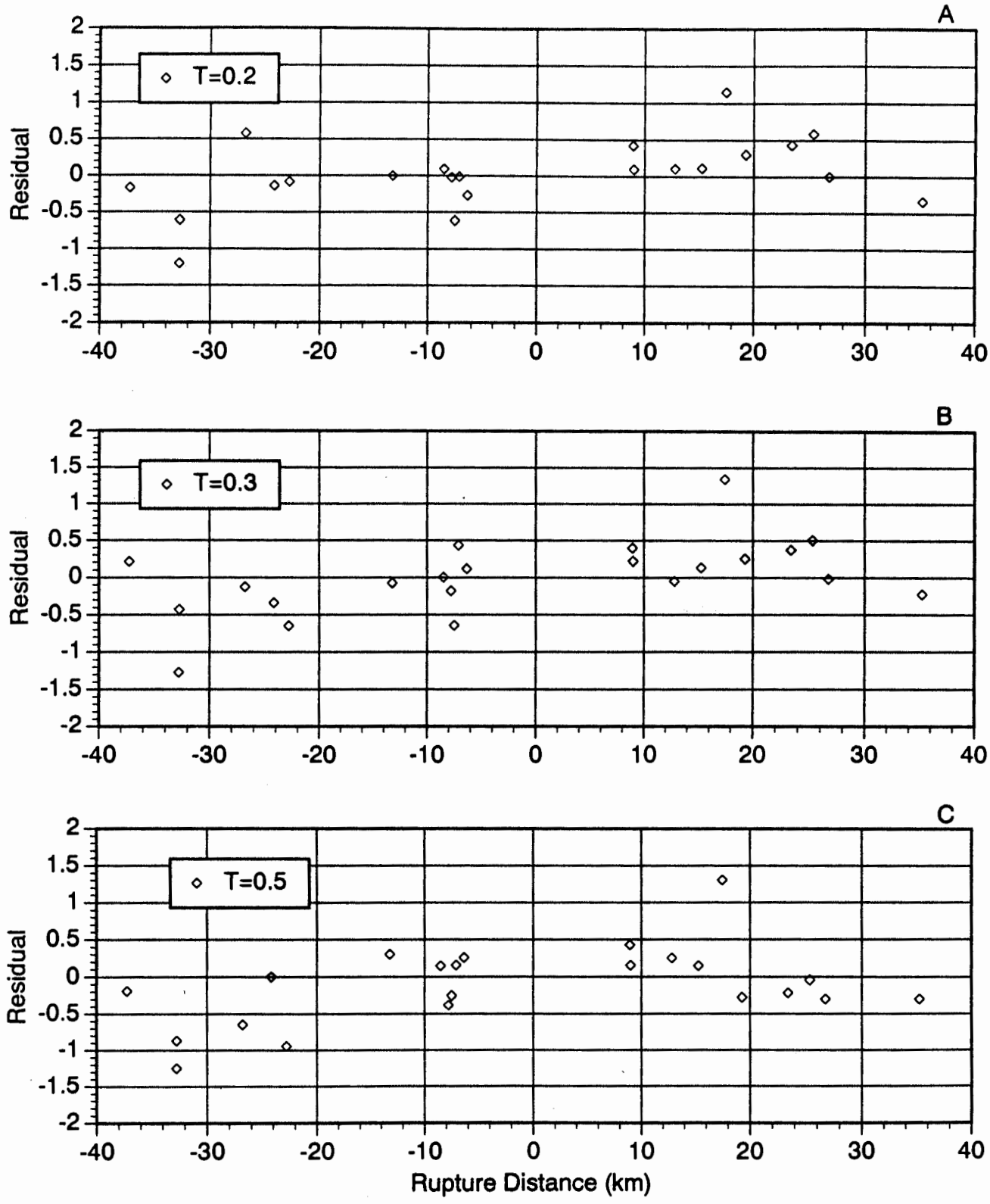

Figure 2-8a. Residuals of the spectral accelerations at 5% damping for sites on the hanging wall (plotted as positive distances) and foot wall (plotted as negative distances). (A) period of 0.2 sec. (B) period of 0.3 sec. (C) period of 0.5 sec.

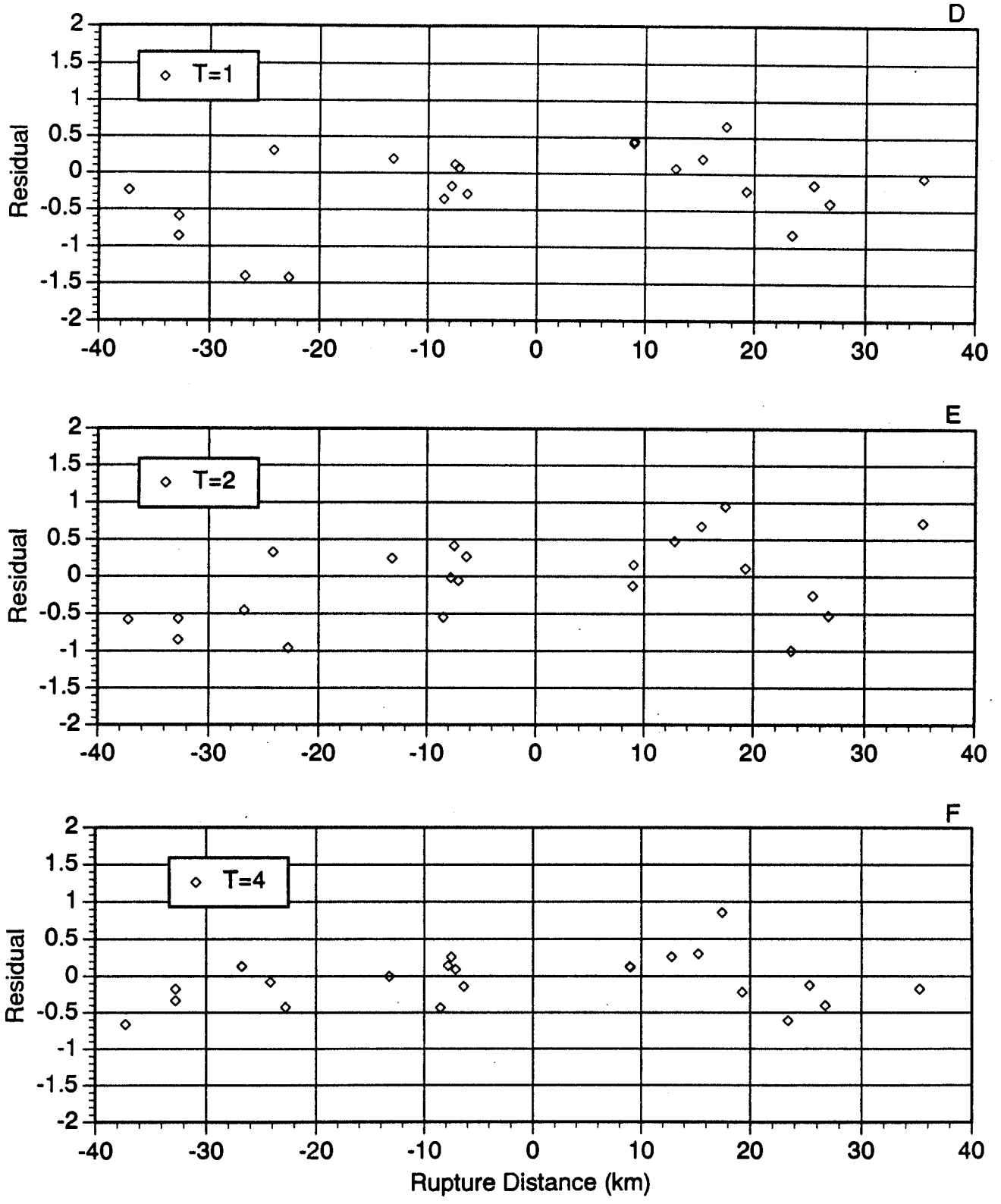

Figure 2-8b. Residuals of the spectral accelerations at 5% damping for sites on the hanging wall (plotted as positive distances) and foot wall (plotted as negative distances). (D) period of 1.0 sec. (E) period of 2.0 sec. (F) period of 4.0 sec.

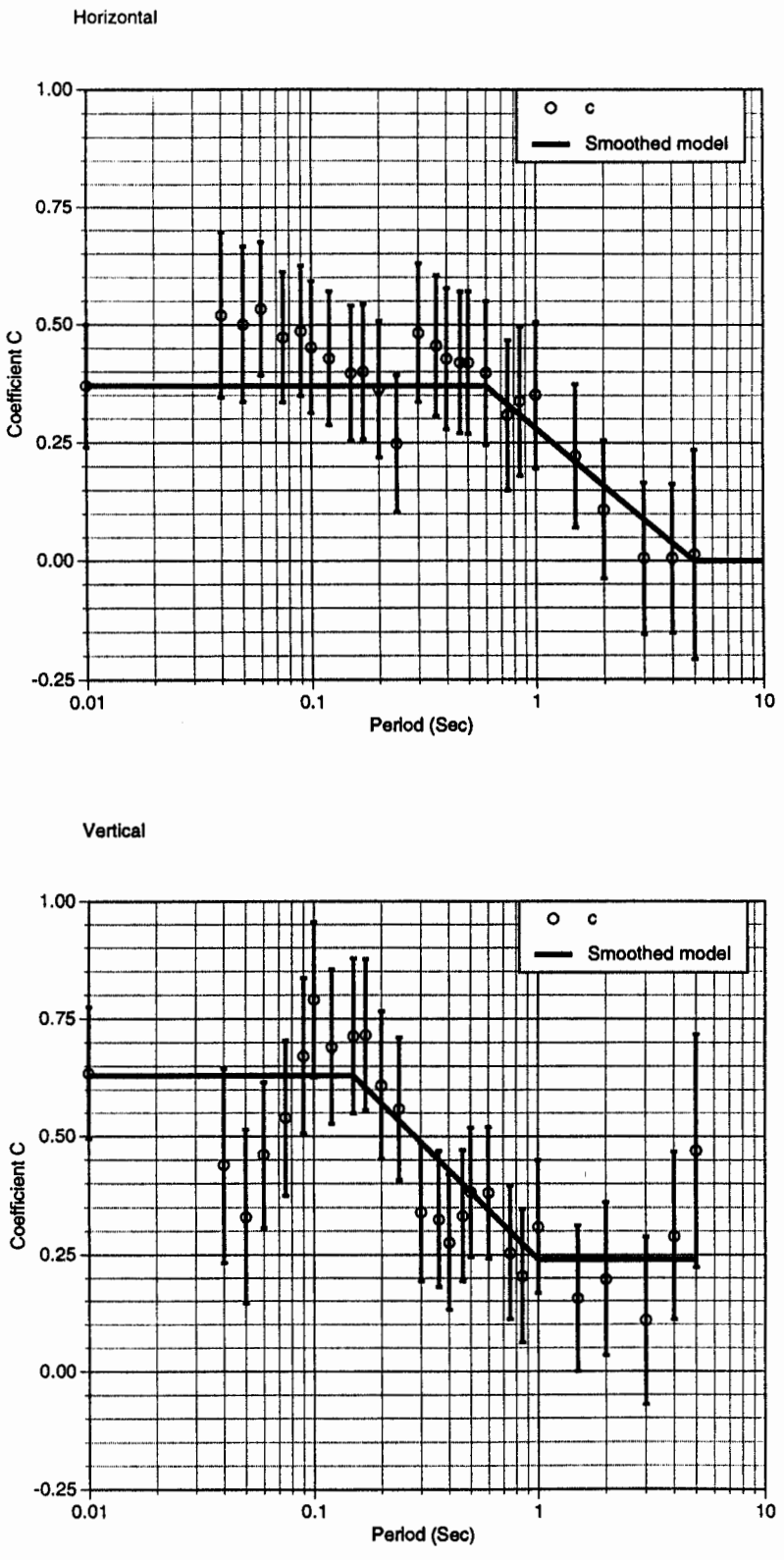

Figure 2-9. Estimated values of coefficient c in Eq (3) as a function of period for the larger data set. The heavy line shows a smoothed model for the period dependence of this coefficient. (A) horizontal component. (B) vertical component.

estimated coefficients are shown by the error bars. On the horizontal component, the maximum hanging wall effect is fairly constant with period (c=0.37) for periods up to about 1 second and then decreases for longer periods, consistent with the trends in the Northridge data. For the vertical component, the hanging wall effect is much larger (c=0.63) for periods up to about 0.2 seconds and then is also decreases for longer periods. The error bars indicate that the hanging wall effect is statistically significant for both the horizontal and vertical components.

A smoothed model of the period dependence of the hanging wall effect is also shown in Figure 2-9. These smoothed coefficients can be used to estimate the ground motions for sites on the hanging wall for future earthquakes. The hanging wall to average ground motion ratios corresponding to these factors are shown in Figure 2-10.

Implications for the Prediction of Ground Motions from Thrust Faults

During the Northridge earthquake, the peak accelerations on the hanging wall were up to 50% higher than the median attenuation at all sites over the limited range of rupture distances of 10 to 20 km. A smaller but similar amplitude has been observed for hanging wall sites from other reverse and reverse/oblique events for the distance range of 5 to 20 km. The data from these other events also indicate that there is a 20% reduction in the peak accelerations on the foot wall over a distance range of 5-20 km; however, this reduction is not observed in the Northridge data. The impact of this effect on peak acceleration attenuation relations is shown in Figure 2-11. This figure shows the average rock site attenuation for Northridge and the attenuation for rock sites on the hanging wall. There were no constraints that the peak acceleration attenuate monotonically with increasing distance. As a result, the peak acceleration on the hanging wall peaks at a rupture distance of 9 km. The fairly flat attenuation from 6 to 12 km on the hanging wall is expected to be a recurring feature of ground motions from reverse events which should be considered in seismic hazard analyses in regions with thrust faults. We expect that a similar effect would be observed for normal faulting events, but there is not enough strong motion data from normal faulting events to test this.

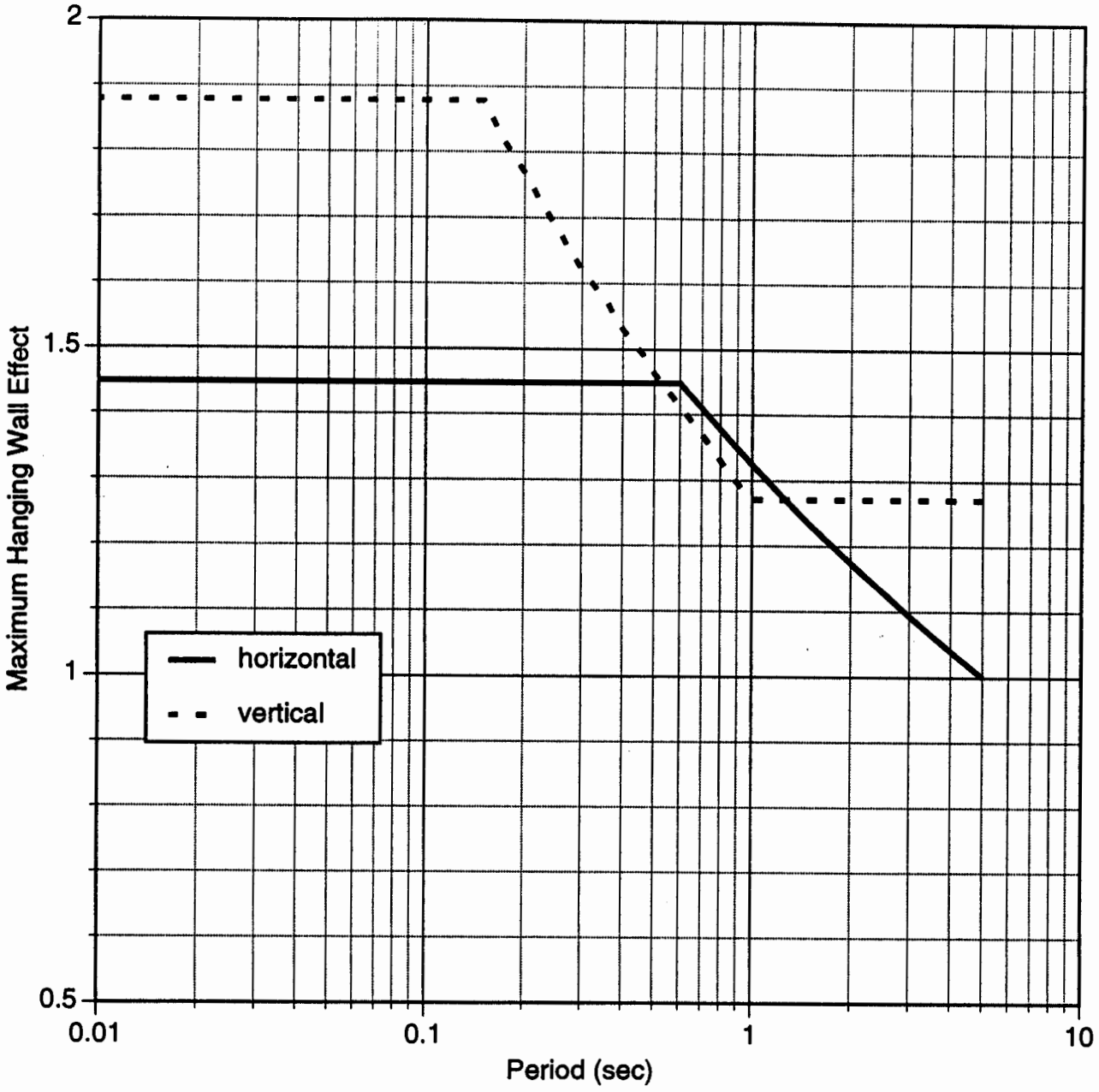

Figure 2-10. Ratio of hanging wall to average ratio as a function of period corresponding to the lines fitted through the data in Figure 2-9.

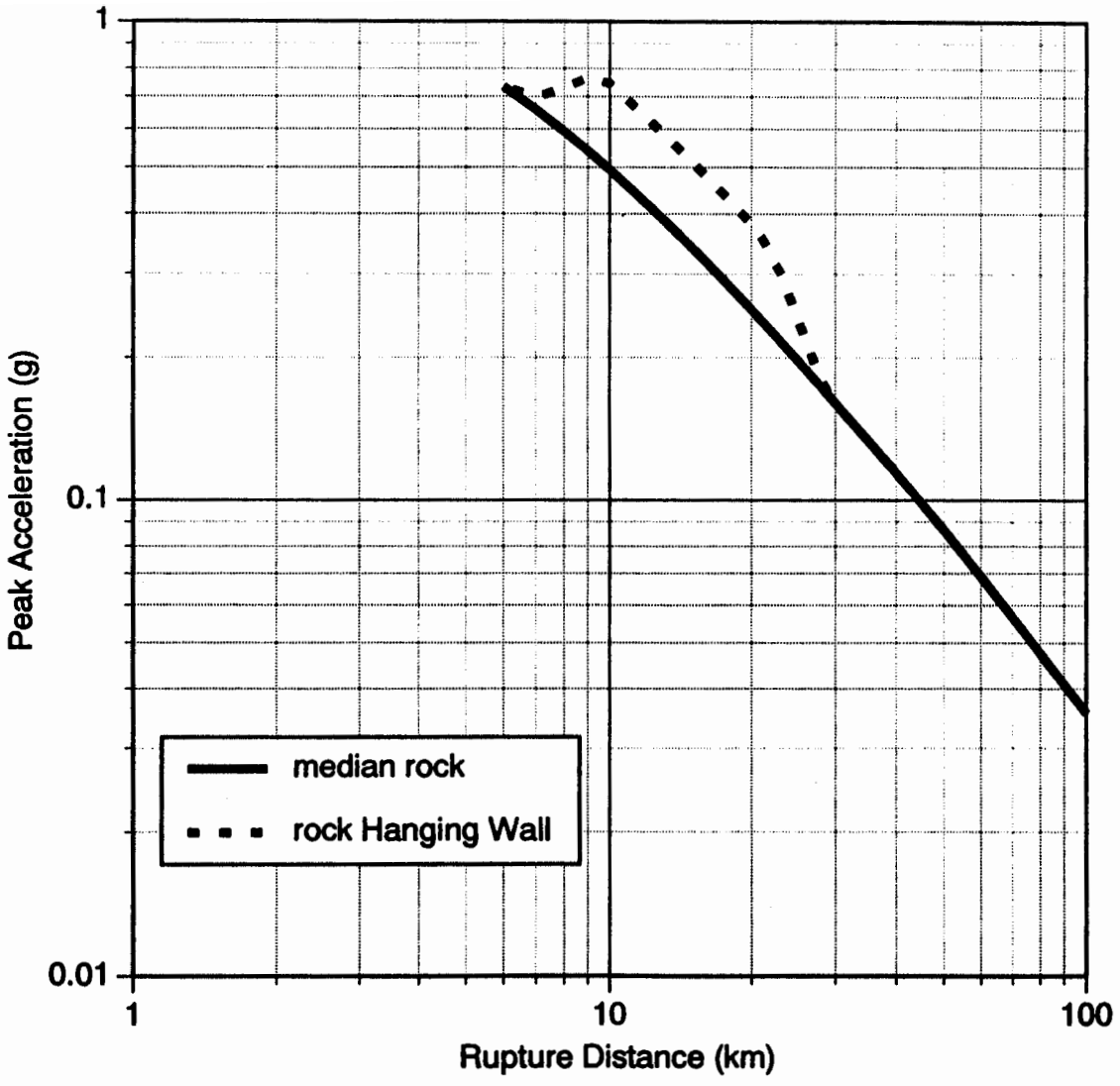

Figure 2-11. Comparison of the regression model peak horizontal acceleration attenuation relations for rock sites and for rock sites located on the hanging wall.

The increase in the peak acceleration on the hanging wall is not due to directivity because as discussed earlier, directivity would have its largest effect on the footwall sites. It is related to the use of the rupture distance as the closest distance measure. If the Boore et al, 1993 distance measure (closest distance to the vertical projection of the rupture surface) is used, it already includes some of the hanging wall effects because sites directly over the hanging wall are all at zero distance.

In this analysis, we have not considered possible dependencies on magnitude, dip angle, or depth to the top of the fault rupture. We expect that the distance range most affected by the hanging wall effect will depend on the dip angle, depth to the top of the fault, and the fault width. In future work, we will use the full data set to examine the dependence of the hanging wall and foot wall effects on these source parameters.

REFERENCES

Abrahamson, N.A., P.G. Somerville, and C. Allin Cornell (1990). Uncertainty in numerical ong motion predictions, *Proc. 4th U.S. National Conference on Earthquake Engineering,,* 1, 407-416.

Abrahamson, N. A. and P. G. Somerville (1993). Estimation of hanging wall and footwall effects on peak acceleration, *Proc. International Workshop on Strong Motion Data,* Menlo Park, California, December 13-17, 1993.

Abrahamson, N.A. and P.G. Somerville (1996). Effects of Hanging Wall and Foot Wall on Ground Motions recorded during the Northridge earthquake, *Bull. Seism. Soc. Am.*, 86, No. 1B, pp. S93-S99.

Abrahamson, N. A. and W. Silva (1997). Empirical response spectral attenuation relations for shallow crustal earthquakes. *Seismological Research Letters* 68, pp. 94-127.

Atkinson, G.M. and P.G. Somerville (1994). Calibration of time history simulation methods. *Bull.Seism. Soc. Am.* 84, 400-414.

Boore, D. M., W. B. Joyner, and T. Fumal (1993). Estimation of response spectra and peak accelerations from western North American earthquakes: an interim report, *U.S. Geological Survey, OFR* 93-509.

Boore, D. M., W. Joyner, and T. Fumal (1997). Equations for estimating horizontal response spectra and peak acceleration from western North American earthquakes: a summary of recent work. *Seismological Research Letters* 68, pp. 128-153.

Campbell, K. W. (1997). Empirical near-source attenuation relationships for horizontal and vertical components of peak ground acceleration, peak ground velocity, and pseudo absolute acceleration response spectra. *Seismological Research Letters* 68, pp. 154-179.

Campbell, K.W. (1995). Preliminary empirical analysis of near-source ground motion from the M_w 6.7 Northridge, California, earthquake of January 17, 1994. *Seismological Research Letters* 66, p. 27.

Campbell, K. W. and Y. Bozorgnia (1994). Near-source attenuation of peak horizontal acceleration from worldwide accelerograms recorded from 1957 to 1993, *Proc. Fifth National Conf. Earthquake Eng.*, III, 283-192.

Graves, R.W. (1994). Preliminary analysis of long-period basin response in the Los Angeles region from the 1994 Northridge earthquake, *Geophysical Research Letters*, 22, 101-104.

Hartzell, S.H. and T.H. Heaton (1983). Inversion of strong ground motion and teleseismic waveform data for the fault rupture of the 1979 Imperial Valley, California earthquake, *Bull. Seism. Soc. Am.* 83, 780-810.

Helmberger, D.V. and D.G. Harkrider (1978). Modeling earthquakes with generalized ray theory, In: J. Miklowitz and J. Achenbach (Editors), *Proc. IUATM Symp. in Modern Problems in Elastic Wave Propagation. Wiley*, New York, pp. 449-518.

Husid, R. (1969). Analisis de teremotos: Analisis General, *Revista IDIEM*, 8, 21-42, Santiago, Chile.

Idriss, I.M. (1991). Selection of earthquake ground motions at rock sites, Report prepared for the Structures Division, Building and Fire Research Laboratory, NIST.

Nigam, N. C., and P. Jennings (1969). Calculation of response spectra from strong motion earthquake records, *Bull. Seism. Soc. Am.*, 909-922.

Porcella, R.L., E.C. Etheridge, R.P. Maley, and A.V. Acosta (1994). Accelerograms recorded at USGS national strong-motion network stations during the Ms = 6.6 Northridge, California earthquake of January 17, 1994, *U.S.G.S. Open File Report 94-141*, 100 pp.

Sadigh, K. (1987). Personal Communication referenced by Joyner and Boore (1988), Ground Motion Prediction, *Proc. ASCE, Earth. Engin. Soil Dyn., II, Recent Advance in Ground Motion Evaluation,* p. 67.

Sadigh, K., C.-Y. Chang, J.A. Egan, F. Makdisi, and R.R. Youngs (1997). Attenuation relationships for shallow crustal earthquakes based on California strong motion data. *Seismological Research Letters* 68, pp. 180-189.

Sadigh, K., C-Y Chang, N. A. Abrahamson, S. J. Chiou, and M. S Power (1993). Specification of long period ground motions: updated attenuation relationships for rock site conditions and adjustment factors for near-fault effects, *Proc. ATC 17-1, Seminar on Seismic Isolation, Passive Energy Dissipation, and Active Control,* Vol I, 59-70.

Saikia, C.K. (1993). Estimated ground motions in Los Angeles due to M=7 earthquake on the Elysian thrust fault, *Bull. Seism. Soc. Am.* 83, 780-810.

Saikia, C.K. (1994a). Modified frequency-wavenumber algorithm for regional seismograms using Filon's quadrature: modeling of Lg waves in eastern North America. *Geophys. J. Int.* 118, 142-158.

Saikia, C.K. (1994b). Modeling of strong ground motions from the 16 September 1978 Tabas, Iran, Earthquake, *Bull. Seism. Soc. Am.* 84, 31-46.

Saikia, C.K., D.S. Dreger, and D.V. Helmberger (1994). Modeling of energy amplification recorded within greater Los Angeles using irregular structure, *Bull. Seism. Soc. Am.* 84, 47-61.

Saikia, C.K. and P.G. Somerville (1995). Influence of slip model, rupture velocity and rise time on the prediction of design ground motions for large earthquakes, Abstract, *Eleventh World Conference on Earthquake Engineering,* Acapulco, Mexico, June 23-28, 1996.

Shakal, A., M. Huang, R. Darragh, T. Cao, R. Sherburne, P. Malhotra, C. Cramer, R.Sydnor, V. Grazier, G. Maldonado, C. Peterson and J. Wampole (1995). Report OSMS 94-07, *California Strong Motion Instrumentation Program*, 308 pp.

Somerville, P.G. (1993). Engineering applications of strong motion simulation, *Tectonophysics*, 218, 195-219.

Somerville, P.G., J.P. McLaren, C.K. Saikia, and D.V. Helmberger (1990). The 25 November, 1988 Saguenay, Quebec earthquake: source parameters and the attenuation of strong ground motion, *Bull. Seism. Soc. Am.* 80, 1118-1143.

Somerville, P.G. and N.A. Abrahamson (1991). Characterizing earthquake slip models for the prediction of strong ground motions, *EOS* 72, 341. (abstract).

Somerville, P.G., M.K. Sen and B.P. Cohee (1991a). Simulation of strong ground motions recorded during the 1985 Michoacan, Mexico and Valaparaiso, Chile earthquakes, *Bull. Seism. Soc. Am.* 81, 1-27.

Somerville, P.G., N.A. Abrahamson, and D.J. Wald (1991b). Characterizing earthquake slip models for the prediction of strong ground motion, unpublished report.

Somerville, P.G. and R.W. Graves (1993). Conditions that give rise to unusually large long period ground motions, *The structural design of tall buildings* 2, 211-232.

Somerville, P.G., N.F. Smith and R.W. Graves (1994a). The effect of critical Moho reflections on the attenuation of strong motion from the 1989 Loma Prieta, in *"The Loma Prieta, California, Earthquake of October 17, 1989 - Strong Ground Motion,"* U.S.G.S. Professional Paper 1551-A, A67-A75.

Somerville, P.G., D.J. Wald, and N.F. Smith (1994b). Prediction of the near-source ground accelerations of the Loma Prieta earthquake using a heterogeneous slip model,

unpublished manuscript.

Somerville, P.G., R.W. Graves, and C.K. Saikia. (1995a). Characterization of Ground Motions at the Sites of Subject Buildings, *Report on Task 4 of the SAC Joint Venture Program for the Reduction of Earthquake Hazards in Steel Moment Frame Buildings.*

Somerville, P.G., R.W. Graves, and N.A. Abrahamson (1995b). Assessment of near-fault rupture directivity effects in the development of design ground motions for Caltrans bridges. *National Seismic Conference on Bridges and Highways, San Diego*, December 10-13, 1995.

Somerville, P. G., C. Saikia, D. Wald, and R. Graves (1966). Implications of the Northridge earthquake for strong ground motions from thrust faults, *Bull. Seism. Soc. Am.* 86, No. 1B, pp. S115-125.

Tognazzini, R., C. Davis and P. Lahr (1995). Data Reports, January 17, 1994 Northridge earthquake.

Trifunac, M.D., M.I. Todorovska, and S.S. Ivanovic (1994). A note on distribution of uncorrected peak ground accelerations during the Northridge, California earthquake of 17 January 1994. *Soil Dynamics and Earthquake Engineering* 13, 187-196.

Wald, D.J. (1992). Rupture characteristics of California earthquakes, Ph.D. Thesis, Seismological Laboratory, California Institute of Technology, 277 pp.

Wald, D.J. and T.H. Heaton (1994). A dislocation model of the 1994 Northridge, California earthquake determined from strong ground motions, *U.S. Geological Survey Open File Report* 94-278.

Wald, D.J., T.H. Heaton and K.W. Hudnut (1996). Slip history of the 1994 Northridge, California earthquake determined from strong motion, teleseismic, GPS, and leveling data, *Bull. Seism. Soc. Am.* 86, No. 1B, pp. S115-125.

Wald, D.J., L.J. Burdick and P.G. Somerville (1988a). Simulation of acceleration time histories close to large earthquakes. *Earthquake Engineering and Soil Dynamics II - Recent Advances in Ground Motion Evaluation*, Geotechnical Special Publication 20, J. Lawrence Von Thun, ed., 430-444.

Wald, D.J., P.G. Somerville and L.J. Burdick (1988b). Simulation of recorded acceler-ations of the 1987 Whittier Narrows earthquake, *Earthquake Spectra* 4, 139-156.

LIST OF CSMIP DATA UTILIZATION REPORTS

California Department of Conservation
Division of Mines and Geology
Office of Strong Motion Studies
California Strong Motion Instrumentation Program (CSMIP)

The California Strong Motion Instrumentation Program (CSMIP) publishes data utilization reports as part of the Data Interpretation Project. These reports were prepared by investigators funded by CSMIP. Results obtained by the investigators were summarized in the papers included in the proceedings of the annual seminar. These reports and seminar proceedings are available from CSMIP at nominal cost. Requests for the reports, seminar proceedings and/or for additional information should be addressed to: Data Interpretation Project Manager, Office of Strong Motion Studies, Division of Mines and Geology, California Department of Conservation, 801 K Street, MS 13-35, Sacramento, California 95814-3531. Phone: (916)322-3105

CSMIP/92-01 **"Evaluation of Soil-Structure Interaction in Buildings during Earthquakes,"** by G. Fenves and G. Serino, June 1992, 57 pp.

CSMIP/92-02 **"Seismic Performance Investigation of the Hayward BART Elevated Section,"** by W. Tseng, M. Yang and J. Penzien, September 1992, 61 pp.

CSMIP/93-01 **"Influence of Critical Moho Reflections on Strong Motion Attenuation in California,"** by P. Somerville, N. Smith and D. Dreger, December 1993, 84 pp.

CSMIP/93-02 **"Investigation of the Response of Puddingstone Dam in the Whittier Narrows Earthquake of October 1, 1987,"** by J. Bray, R. Seed and R. Boulanger, December 1993, 60 pp.

CSMIP/93-03 **"Investigation of the Response of Cogswell Dam in the Whittier Narrows Earthquake of October 1, 1987,"** by R. Boulanger, R. Seed and J. Bray, December 1993, 53 pp.

CSMIP/94-01 **"Torsional Response Characteristics of Regular Buildings under Different Seismic Excitation Levels,"** by H. Sedarat, S. Gupta, and S. Werner, January 1994, 43 pp.

CSMIP/94-02 **"Degradation of Plywood Roof Diaphragms under Multiple Earthquake Loading,"** by J. Bouwkamp, R. Hamburger and J. Gillengerten, February 1994, 32 pp.

CSMIP/94-03 **"Analysis of the Recorded Response of Lexington Dam during Various Levels of Ground Shaking,"** by F. Makdisi, C. Chang, Z. Wang and C. Mok, March 1994, 60 pp.

CSMIP/94-04 **"Correlation between Recorded Building Data and Non-Structural Damage during the Loma Prieta Earthquake of October 17, 1989,"** by S. Rihal, April 1994, 65 pp.

LIST OF CSMIP DATA UTILIZATION REPORTS (continued)

CSMIP/94-05 **"Simulation of the Recorded Response of Unreinforced Masonry (URM) Infill Buildings,"** by J. Kariotis, J. Guh, G. Hart and J. Hill, October 1994, 149 pp.

CSMIP/95-01 **"Seismic Response Study of the Hwy 101/Painter Street Overpass Near Eureka Using Strong-Motion Records,"** by R. Goel and A. Chopra, March 1995, 70 pp.

CSMIP/95-02 **"Evaluation of the Response of I-10/215 Interchange Bridge Near San Bernardino in the 1992 Landers and Big Bear Earthquakes,"** by G. Fenves and R. Desroches, March 1995, 132 pp.

CSMIP/95-03 **"Site Response Studies for Purpose of Revising NEHRP Seismic Provisions,"** by C.B. Crouse, March 1995, 68 pp.

CSMIP/96-01 **"An Investigation of UBC Serviceability Requirements from Building Responses Recorded During the 1989 Loma Prieta Earthquake,"** by C.-M. Uang and A. Maarouf, September 1996, 140 pp.

CSMIP/96-02 **"Evaluation of Displacement Amplification Factor for Seismic Design Provisions,"** by C.-M. Uang and A. Maarouf, September 1996, 167 pp.

CSMIP/00-01 **"Prediction of Ground Motions for Thrust Earthquakes,"** by Paul Somerville and Norman Abrahamson, February 2000, 56 pp.

SMIP89 "SMIP89 Seminar on Seismological and Engineering Implications on Recent Strong-motion Data," Preprints, Sacramento, California, May 9, 1989

SMIP90 "SMIP90 Seminar on Seismological and Engineering Implications on Recent Strong-motion Data," Preprints, Sacramento, California, June 8, 1990

SMIP91 "SMIP91 Seminar on Seismological and Engineering Implications on Recent Strong-motion Data," Preprints, Sacramento, California, May 30, 1991

SMIP92 "SMIP92 Seminar on Seismological and Engineering Implications on Recent Strong-motion Data," Proceedings, Sacramento, California, May 21, 1992

SMIP93 "SMIP93 Seminar on Seismological and Engineering Implications on Recent Strong-motion Data," Proceedings, Sacramento, California, May 20, 1993, 114 pp.

SMIP94 "SMIP94 Seminar on Seismological and Engineering Implications on Recent Strong-motion Data," Proceedings, Los Angeles, California, May 26, 1994, 120 pp.

SMIP95 "SMIP95 Seminar on Seismological and Engineering Implications on Recent Strong-motion Data," Proceedings, San Francisco, California, May 16, 1995, 105 pp.

SMIP96 "SMIP96 Seminar on Seismological and Engineering Implications on Recent Strong-motion Data," Proceedings, Sacramento, California, May 14, 1996, 130 pp.

LIST OF CSMIP DATA UTILIZATION REPORTS (continued)

SMIP97	"SMIP97 Seminar on Utilization of Strong-Motion Data," Proceedings, Los Angeles, California, May 8, 1997, 127 pp.
SMIP98	"SMIP98 Seminar on Utilization of Strong-Motion Data," Proceedings, Oakland, California, September 15, 1998, 175 pp.
SMIP99	"SMIP99 Seminar on Utilization of Strong-Motion Data," Proceedings, Los Angeles, California, September 15, 1999, 154 pp.